# Insight into Selected Reactions in Low-Temperature Dimethyl Ether Combustion from Born−Oppenheimer Molecular Dynamics†

**Amity Andersen**

*Accelrys, Inc., 10188 Telesis Court, Suite 100, San Diego, California, 92121*

**Emily A. Carter***

*Department of Mechanical and Aerospace Engineering and Program in Applied and Computational Mathematics, Princeton University, Princeton, New Jersey 08544-5263*

*Received: August 11, 2005; In Final Form: October 28, 2005*

Dimethyl ether is under consideration as an alternative diesel fuel. Its combustion chemistry is as yet ill-characterized. Here we use Born−Oppenheimer molecular dynamics (BOMD) based on DFT-B3LYP forces to investigate the short-time dynamics of selected features of the low-temperature dimethyl ether (DME) oxidation potential energy surface. Along the chain propagation pathway, we run BOMD simulations from the transition state involving the decomposition of $^{\bullet}CH_2OCH_2OOH$ to two $CH_2{=}O$ and an $^{\bullet}OH$ radical. We predict that formaldehyde C−O stretch overtones are excited, consistent with laser photolysis experiments. We also predict that O−H overtones are excited for the $^{\bullet}OH$ formed from $^{\bullet}CH_2OCH_2OOH$ dissociation. We also investigate short-time dynamics involved in chain branching. First, we examine the isomerization transition state of $^{\bullet}OOCH_2OCH_2OOH \rightarrow HOOCH_2O\dot{C}HOOH$. The latter species is predicted to be a short-lived metastable radical that decomposes within 500 fs to hydroperoxymethyl formate (HPMF; $HOOCH_2OC(=O)H$) and the first $^{\bullet}OH$ of chain branching. The dissociation of $HOOCH_2O\dot{C}HOOH$ exhibits non-RRKM behavior in its lifetime profile, which may be due to conformational constraints or slow intramolecular vibrational energy transfer (IVR) from the nascent H−O bond to the opposite end of the radical, where O−O scission occurs to form HPMF and $^{\bullet}OH$. In a few trajectories, we see $HOOCH_2O\dot{C}HOOH$ recross back to $^{\bullet}OOCH_2OCH_2OOH$ because the isomerization is endothermic, with only an 8 kcal/mol barrier to recrossing. Therefore, some inhibition of chain-branching may be due to recrossing. Second, trajectories run from the transition state leading to the direct decomposition of HPMF (an important source of the second $^{\bullet}OH$ radical in chain branching) to $H\dot{C}O$, $^{\bullet}OH$, and $HC(=O)OH$ show that these products can recombine to form many other possible products. These products include $CH_2OO + HC(=O)OH$, $H_2O + CO + HC(=O)OH$, $HC(=O)OH + HC(=O)OH$, and $HC(=O)C(=O)H + H_2O$, which (save $CH_2OO + HC(=O)OH$) are all more thermodynamically stable than the original $H\dot{C}O + {}^{\bullet}OH + HC(=O)OH$ products. Moreover, the multitude of extra products suggest that standard statistical rate theories cannot completely describe the reaction kinetics of significantly oxygenated compounds such as HPMF. These secondary products consume the second $^{\bullet}OH$ required for explosive combustion, suggesting an inhibition of DME fuel combustion is likely.

## I. Introduction

With ever more stringent restrictions being placed on the emissions of air pollutants such as $NO_x$ and particulate matter around the world, the need for clean-burning alternative sources of energy becomes more pressing. Dimethyl ether (DME) has been proposed as a replacement for conventional diesel fuel. DME's propensity to compression ignite is comparable to that of conventional diesel fuel, which is comprised of long-chain hydrocarbons. Unlike conventional diesel fuel, DME creates little soot when combusted at relatively low temperatures. This "soot-free" property has been attributed to DME's lack of carbon−carbon bonds in its molecular structure, which inhibits soot aggregation.[1] Dimethyl ether also has a number of other desirable properties such as low toxicity and low photoactivity. DME can also be produced economically in a single-step synthesis process, and current liquid petroleum gas (LPG) technology can form a basis for future DME storage and infrastructure.[2]

The mechanism for low-temperature autoignition has been modeled after analogous mechanisms for low-temperature oxidation of long-chain hydrocarbons.[3] This mechanism involves chain branching, in which there is an exponential increase in the number of highly reactive radicals (e.g., $^{\bullet}OH$, $HOO^{\bullet}$, etc.). A basic schematic representation of DME's primary low-temperature chain mechanism pathways based on our previous calculations[4,5] is shown in Figure 1. Labeling of the transition state barriers follows the labeling scheme of our previous work.[4,5] The mechanism begins with $O_2$ addition to $CH_3O\dot{C}H_2$ radical, which has been formed via hydrogen abstraction from $CH_3OCH_3$ in the initiation step. The most probable species involved in hydrogen abstraction from $CH_3OCH_3$ are $O_2$ (initial oxidation), $HOO^{\bullet}$, and $^{\bullet}OH$ (the most reactive). Two paths are represented in Figure 1: a chain propagation path in which one $^{\bullet}OH$ is formed and a chain-branching path in which two $^{\bullet}OH$ are formed. Chain-branching begins when $^{\bullet}CH_2OCH_2OOH$ is

† Part of the special issue "William Hase Festschrift".

* Corresponding author. E-mail: eac@princeton.edu.

10.1021/jp054509y CCC: $33.50 
Published on Web 12/09/2005

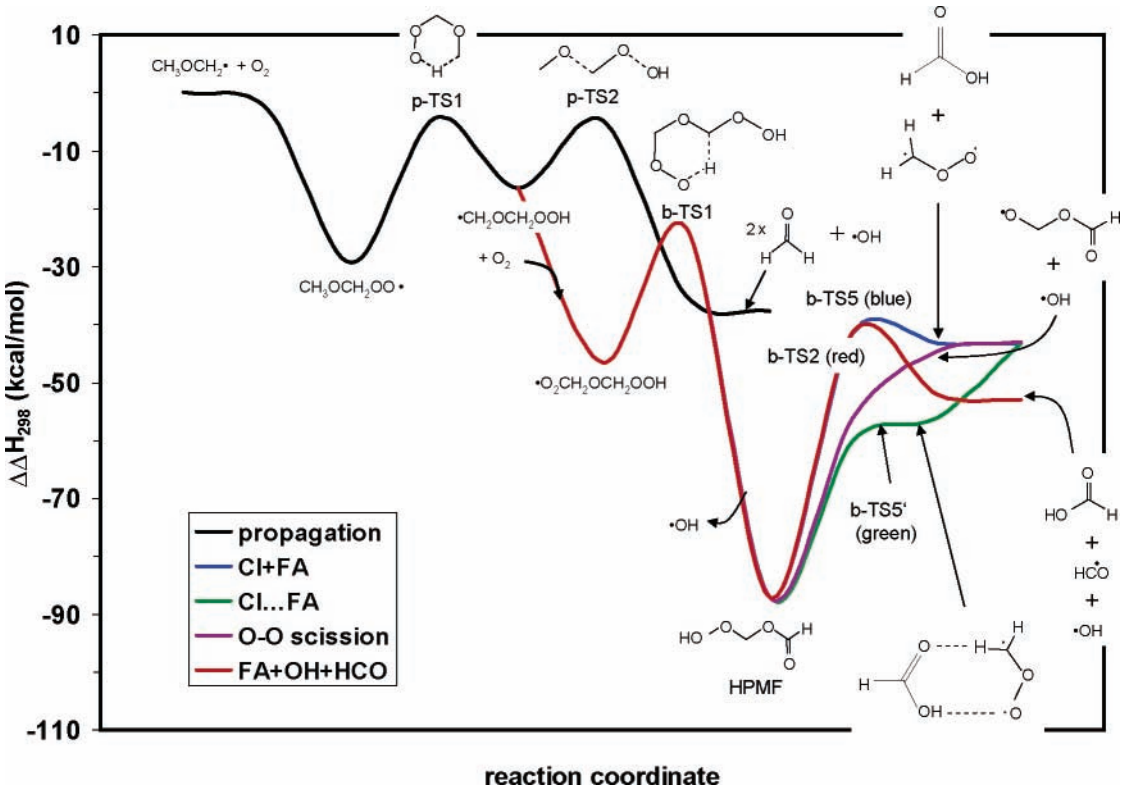


**Figure 1.** Schematic of the dimethyl ether potential energy surface according to DFT-B3LYP//6-311G* from our previous work.[4] "CI" stands for the Criegee intermediate of ethylene ozonolysis, and "FA" stands for formic acid.

diverted from the propagation path via a collision with $O_2$ to form $^{\bullet}OOCH_2OCH_2OOH$. If $^{\bullet}OOCH_2OCH_2OOH$ does not dissociate back into its precursors, it can undergo reactions that ideally lead to the production of two highly reactive $^{\bullet}OH$ radicals.

As we have shown previously,[5] the chain-branching intermediate hydroperoxymethyl formate ($HOOCH_2OC(=O)H$, HPMF) has several possible dissociation channels that do not necessarily lead to the formation of a second $^{\bullet}OH$ radical. For simplicity, Figure 1 shows only the four lowest energy reaction paths. The lowest energy path leads to the formation of a hydrogen-bonded complex of carbonyl oxide (the Criegee intermediate of ethylene ozonolysis) and formic acid. A second path shown in Figure 1 (in blue) leads to noncomplexed carbonyl oxide and formic acid. The Criegee intermediate can decompose into $^{\bullet}OH$ and other products unimolecularly[6−15] or bimolecularly.[16−29] The second lowest energy path is the formation of the radicals $^{\bullet}OCH_2OC(=O)H$ and $^{\bullet}OH$ via scission of the O−O bond in HPMF. The fourth lowest energy path shown in Figure 1 directly leads to $^{\bullet}OH$ radical along with $H\dot{C}O$ and $HC(=O)$-OH. The barrier to this reaction is comparable to that for producing noncomplexed carbonyl oxide and formic acid.[4,5] Both direct $^{\bullet}OH$ and formic acid formation and noncomplexed $CH_2OO$ and $HC(=O)OH$ formation are energetically[5] and kinetically[30] unfavorable compared with the O−O scission and $CH_2OO\cdots HC(=O)OH$ complex formation pathways.

Experimental data are sparse for low-temperature DME oxidation. The most thorough studies of the kinetics of the chain propagation pathway (black curve in Figure 1) were done by Sehested et al.[31] and Maricq et al.[32] Sehested et al. used indirect methods (smog chamber with detailed kinetics modeling) while Maricq et al. employed laser photolysis techniques to derive their respective kinetics data. Both studies were conducted in conditions below and around atmospheric (1 atm and 298 K). Since Maricq et al. performed their experiments in real time, they were able to observe a dynamical aspect of the dissociating $^{\bullet}CH_2OCH_2OOH$ radical. They noted that their rate of dissociating $^{\bullet}CH_2OCH_2OOH$ derived from observed formaldehyde formation was about two times lower than the rates determined indirectly through measuring $CH_3O\dot{C}H_2$ loss and $CH_3OCH_2$-$OO^{\bullet}$ formation with time-resolved UV spectroscopy. They reasoned that $CH_2{=}O$ was produced vibrationally excited due to the ~40 kcal/mol excess energy from the reactants, $CH_3O\dot{C}H_2$ + $O_2$. They measured $CH_2{=}O$ formation with a diode laser that probed the $v = 0 \rightarrow v = 1$ transition of the $CH_2{=}O$ carbonyl stretching mode. Thus, $CH_2{=}O$ with a vibrationally excited C−O stretch would be "transparent" to their diode laser probe when formed from $^{\bullet}CH_2OCH_2OOH$. The excited $CH_2{=}O$ would then relax via collisions and would be visible to the probe only at later times. The present work will provide theoretical evidence in support of this proposal.

Even less is known about the chain branching pathway. Experiments of Curran et al.,[3,33] Dagaut et al.,[34] and Liu et al.[35] represent the only experimental (with detailed kinetics modeling) studies addressing the low-temperature chain-branching mechanism of DME. The most thorough of these studies of the low-temperature chain-branching mechanism is that of Curran et al.[3,33] These studies, however, only give direct information about stable product yields. Mechanistic details of DME combustion must be inferred from stable product yields within a comprehensive kinetics model. These studies do not explore possible dynamics issues that may occur in the low-temperature chain mechanism. Thus, the aim of the present work is to probe areas of the DME chain reaction mechanism potential energy surface where short-time dynamics may yield insight into behavior that cannot be predicted by standard statistical rate theories (e.g., conventional transition state theory (CTST) and RRKM theory). As we shall see, the reaction dynamics we observe indicates a mechanistic complexity in the combustion of DME not anticipated from such statistical kinetics theories.

## II. Theoretical Method

**A. Electronic Structure Details.** Absolute energies, optimized structures, and harmonic frequencies for the systems considered here were calculated in our previous work.[4,5] Born−Oppenheimer molecular dynamics treats the motion of the nuclei classically with Newton's equations. However, the light mass of hydrogen in general should not be treated with classical dynamics. Deuterium is typically heavy enough to be treated classically. Therefore, to minimize the error in the classical dynamics used to propagate the nuclei due to neglecting quantum effects of light hydrogens, we have replaced all hydrogens with deuterium. Though good direct dynamics results have been attained for direct reactions of hydrogenated H + $H_2$[36] and hydrogenated trimethylene,[37−39] H + $H_2$ is much smaller than our systems, which have 24−30 degrees of freedom, and the primary focus of Doubleday and co-workers' trimethylene work was to determine branching ratios of the conrotatory and disrotatory rotation of the methylene ends formed in cyclopropane ring-breaking.[37−39] Most of our systems involve hydrogen transfer between heavy carbon and oxygen atoms, which occurs either directly from the transition state or indirectly later on in the trajectory. Zero-point energy flow is a problem for high frequency O−H and C−H stretches, hence our use of deuterium instead of hydrogen. Our results may be viewed as only qualitatively correct for hydrogenated species and as predictions for deuterated experiments that may one day be performed. Though deuterium was used in all molecular dynamics simulations presented here, hydrogen atom notation is used in all chemical formulas to prevent confusion.

These calculations were performed using spin-polarized (unrestricted, U) density functional theory (DFT) employing the B3LYP hybrid exchange-correlation functional[40] with the 6-31G** basis set[41,42,43] within the Jaguar ab initio code.[44] Though geometries are available from our previous work using a larger 6-311G** basis set (which may more accurately portray the thermochemistry),[45] running trajectories with 10−12 atoms with the larger basis set would be computationally prohibitive. Thus, all single-point energy/gradient calculations for each molecular dynamics time step were computed at the DFT-B3LYP/6-31G** level of theory. Tables comparing our previous 6-31G** and 6-311G** results may be found in our earlier work.[4,5] The Hessian (energy second derivative matrix) eigenvalues and eigenvectors from a subsequent harmonic frequency analysis were extracted to select initial conditions for the molecular dynamics trajectories, which will be discussed in the next section.

Spin contamination in unrestricted DFT is considerably less than in other unrestricted electronic structure methods, such as unrestricted Hartree−Fock (HF) and unrestricted Møller−Plesset perturbation theory (e.g., MP2, MP4). For the open-shelled systems considered in this study, the highest spin contamination was seen for the p-TS2 transition state. Instead of $\langle S^2 \rangle = 0.75$ for a pure doublet system, we find a value of 0.773 for p-TS2 (3% spin contamination). DFT's lower spin contamination with respect to unrestricted wave function-based theories is a consequence of electron correlation being incorporated through the exchange-correlation functional. Pople and co-workers have asserted that "spin contamination" is not even well-defined for DFT.[46] DFT's formalism is laid out in terms of a density and not a wave function, and Pople et al. argue that real systems can display spin polarization. Moreover, bond dissociation is often well described by UDFT. For example, the O−H bond dissociation of water, where $H_2O$ goes from a singlet species to two doublet species ($H^{\bullet}$ and $^{\bullet}OH$) is well-described by UDFT-B3LYP and does almost as well as the multireference complete active space SCF (CASSCF) level of theory.[47]

The mean average error in the thermochemistry of DFT-B3LYP has been reported to be 3-5 kcal/mol.[48,47] However, this mean average error covers standard systems where experimental heats of formation are well-known (e.g., $H_2O$, $C_2H_6$). By contrast, only some bond energies of peroxy radical and peroxide species (HOO, HOOH, $CH_3OOH$, $CH_3OO$, $CH_3CH_2OOH$, and $CH_3CH_2OO$) have been measured; in these cases, we have found that the error is higher, with a mean average error of 5−9 kcal/mol depending on the system and basis set.[49] Furthermore, we have found in the analogous ethyl radical + $O_2$ system, that the mean error with respect to known experimental thermochemistry derived from kinetics data is 6−7 kcal/mol.[49] One might then suggest that a "more accurate" ab initio theory should be employed. In both the peroxy radical/peroxide bond energies and the ethyl + $O_2$ studies, the corresponding coupled cluster with single, double, and perturbative triple excitations (CCSD(T))[50] results have average errors only 0.2−1 kcal/mol more accurate than those of DFT-B3LYP. Thus, there is little accuracy gain in applying the much more computationally demanding CCSD(T) method over the DFT-B3LYP method. The only methods that claim to attain chemical accuracy (i.e., 1−2 kcal/mol) are the Gaussian-2 (G2)[51] and the complete basis set (CBS)[52] methods. These are heuristic methods comprised of additive terms from a number of ab initio methods (e.g., HF, MP2, QCISD(T)). G2 and CBS only calculate the single-point energy of a given system and rely on the optimized geometries from other methods such as HF, MP2, and DFT-B3LYP. Therefore, G2 and CBS do not calculate gradients and cannot be used in BOMD to calculate forces on the nuclei. Therefore, we concluded that DFT-B3LYP is the best option currently available for use in BOMD simulations.

**B. Molecular Dynamics Initial Conditions.** The Hessian information from electronic structure calculations mentioned above was used in a subsequent random selection of momenta and positions calculated with a code written in our group implementing the quasiclassical normal mode sampling developed by Hase and co-workers.[53,54] In this method, the system is treated as an ensemble of harmonic oscillators, and energy is distributed among the normal modes. Each normal mode is given energy based on a suitable probability distribution. In this work, we selected the energy for each normal mode according to the harmonic quantum Boltzmann distribution $P_i = \exp(-n_i h\nu_i/k_B T)[1 - \exp(-h\nu_i/k_B T)]$, where $n_i$ is the number of quanta of the $i$th mode, $h$ is Planck's constant, $\nu_i$ is the frequency of the $i$th mode (computed from the Hessian eigenvalues), $k_B$ is Boltzmann's constant, and $T$ is the temperature.[55] Due to the locally high barriers along the combustion pathway, all trajectories were started from transition state structures so that rare event dynamics could be studied. The momentum selected along the reaction coordinate is chosen at random using $p_{rc} = \pm[-2k_B T \ln(1 - R)]^{1/2}$, where $R$ is a uniform random number.[56] The Hessian eigenvector matrix is used to make the necessary transformation from internal to Cartesian coordinates and momenta. For finite displacements, the harmonic normal mode approximation is not exact; thus, the selected nuclear velocities and coordinates are rescaled to the desired energy (within 0.1%).[37] The angular momentum of the system was set to $J = 0$ for all trajectories. Spurious angular momentum was removed iteratively with the rescaling of the energy prior to initiating each trajectory. Though selection of angular momentum according to a thermal distribution may be important in modeling possible Coriolis effects,[57] the angular momentum of all

trajectories was set to $J = 0$ for simplicity. The effects of angular momentum are expected to be small compared to that of the internal vibrational energy. At 600 K, the equipartition theorem predicts an average classical total rotational energy of $^3/_2RT =$ 1.8 kcal/mol, which is much smaller than the zero point and thermal vibrational energy of the 10 and 12 atom molecules considered here. Indeed, in ClONO (a much smaller system than those considered here) isomerization/dissociation molecular dynamics simulations, Peña-Gallego et al.[58] found little change in rate constants and branching ratios when 1−2 kcal/mol of rotational energy was added to any of the ClONO's principal axes.

Temperatures for the selection of initial momenta and coordinates for each transition state were chosen based on whether the transition state belonged to the chain-propagation or the chain-branching mechanism. For chain-propagation transition states (p-TS2), a temperature of 300 K was chosen for initialization of the velocities and coordinates. This temperature is within the range of the experiments of Maricq et al.[32] (296−350 K); again, their study addresses dynamical aspects of formaldehyde and •OH production from $CH_3OCH_2 + O_2$. For transition states involved in chain branching (i.e., b-TS1, b-TS2, b-TS5, and b-TS5′), a temperature of 600 K was chosen. This temperature is in the range of peak low-temperature yield of the chain-branching product formic acid observed in the experiments of Liu et al.[35] and Curran et al.[33]

**C. Trajectory Integration.** The velocity−Verlet algorithm of Swope et al.[59] was used to integrate Newton's equations of motion for microcanonical (constant *N*, *V*, *E*) dynamics. The time step for all these calculations was 10 atomic time units (∼0.242 fs). The duration of each trajectory varied, depending on which part of the potential surface we were considering. Trajectories from p-TS2, b-TS2, b-TS5, and b-TS5′ (see Figure 1), each ran for 1 ps. Ten trajectories were executed for the simulation of $•CH_2OCH_2OOH$ dissociation from p-TS2, 30 trajectories for the dissociation of HPMF (deuterated) through b-TS2, and 10 each for the dissociation of HPMF (deuterated) through b-TS5 and through b-TS5′. For the trajectories from b-TS1, a duration of 500 fs was determined from preliminary trajectories to be sufficient for the dissociation of $HOOCH_2O\dot{C}HOOH$. Then 70 trajectories were followed for the isomerization of $•OOCH_2OCH_2OOH$ to $HOOCH_2O\dot{C}HOOH$ through b-TS1. For the trajectories that started from b-TS2, if a trajectory ran from this transition state did not fully react to form products within 1 ps, the trajectory was allowed to run for an additional 1 ps. Velocities for each trajectory were reversed to also verify the backward path toward the reactants.

**D. Analysis.** Viewing of nuclear motion for all trajectories, along with creation of movie snapshots for the progression of the nuclei, were done with XMakeMol.[60] The velocity autocorrelation functions for each of the C−O bonds in the two $CH_2$═O fragments and the O−H bond in •OH fragment formed from $•CH_2OCH_2OOH$ dissociation via p-TS2 were calculated for each of the 10 trajectories starting from p-TS2. The velocity autocorrelation functions for each the C−O bonds in the two formaldehyde fragments and •OH O−H bond were averaged over the 10 trajectories. The Fourier transform of these three average velocity autocorrelation functions were performed using the XmGrace plotting package,[61] yielding power spectra for each of the three bonds (C−O #1, C−O #2, and the O−H).

A "lifetime" curve was constructed by counting the number of $HOOCH_2O\dot{C}HOOH$ that had not dissociated to HPMF (deuterated) and •OH by a given time. For dissociation of $HOOCH_2O\dot{C}HOOH$ via b-TS1, $HOOCH_2O\dot{C}HOOH$ was defined to be dissociated when the breaking O−O bond irreversibly lengthens beyond 2.0 Å. Adjusting this criterion by a few tenths of an angstrom results in about a 5 fs recession or advancement of the lifetime of the $HOOCH_2O\dot{C}HOOH$, but this adjustment is unlikely to change the qualitative behavior of the lifetime plot. Nonlinear curve fitting of this lifetime of the $HOOCH_2O\dot{C}HOOH$ short-lived intermediate formed through b-TS1 was done using the XmGrace plotting package.[61]

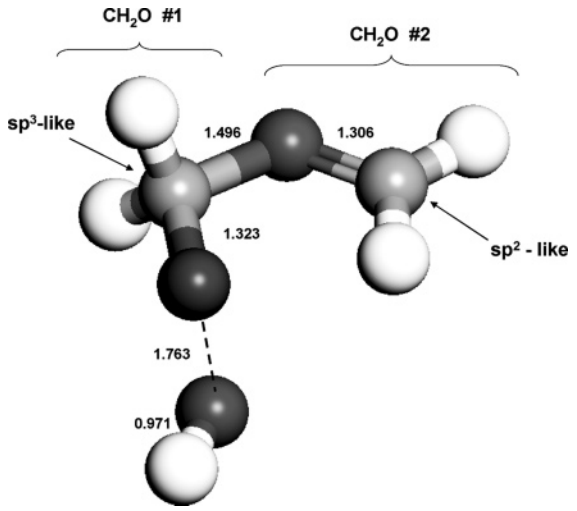


**Figure 2.** Structure of p-TS2. The dark gray balls are oxygen atoms, the light gray balls are carbon atoms, and the white balls are hydrogen atoms. Note the hybridization of the two carbon atoms. Bond lengths are given in Å.

## III. Results and Discussion

**A. Trajectories from p-TS2: chain propagation to produce formaldehyde and •OH.** In our previous work,[4] we located a viable transition state (p-TS2) leading to the dissociation of $•CH_2OCH_2OOH$ to two $CH_2$═O molecules and an •OH radical. Preliminary kinetics work indicates that this DFT-B3LYP barrier may be 3−5 kcal/mol lower than required for sufficient accumulation of $•CH_2OCH_2OOH$ for chain branching ("sufficient" according to experiment).[30] This may affect the quantitative results, but one can still gather some qualitative insight into the dissociation process of $•CH_2OCH_2OOH$. Unfortunately, no other ab initio quantum chemistry method we tried (including multireference configuration interaction and coupled cluster theory, CCSD(T)) was able to reduce the mean average error in energetics beyond the accuracy of DFT-B3LYP.

According to Hammond's postulate, p-TS2 should be reactant-like (see Figure 1), but the O−O bond in p-TS2 is very long (1.763 Å), almost nonexistent. In contrast, the C−O bond between the $CH_2$═O fragments is fairly intact at the saddle point (1.496 Å). Both the damped dynamics simulations (an approximation of the IRC path where the system is very slowly allowed to descend into the reaction and product minima) performed previously[4] and the molecular dynamics performed here indicate that the C−O bond breaks almost immediately after the saddle point. Interestingly, these $CH_2$═O fragments break away with their molecular planes perpendicular to each other (see Figure 2). Consequently, the terminal $CH_2$═O fragment, as it breaks away from the internal $CH_2$═O, rotates about the axis perpendicular to its molecular plane. The internal $CH_2$═O rotates about the axis perpendicular to the C═O bond and parallel to the molecular plane. The radical end already has its $•CH_2$ close to an $sp^2$ configuration. When the formaldehyde fragments are formed almost instantaneously after the

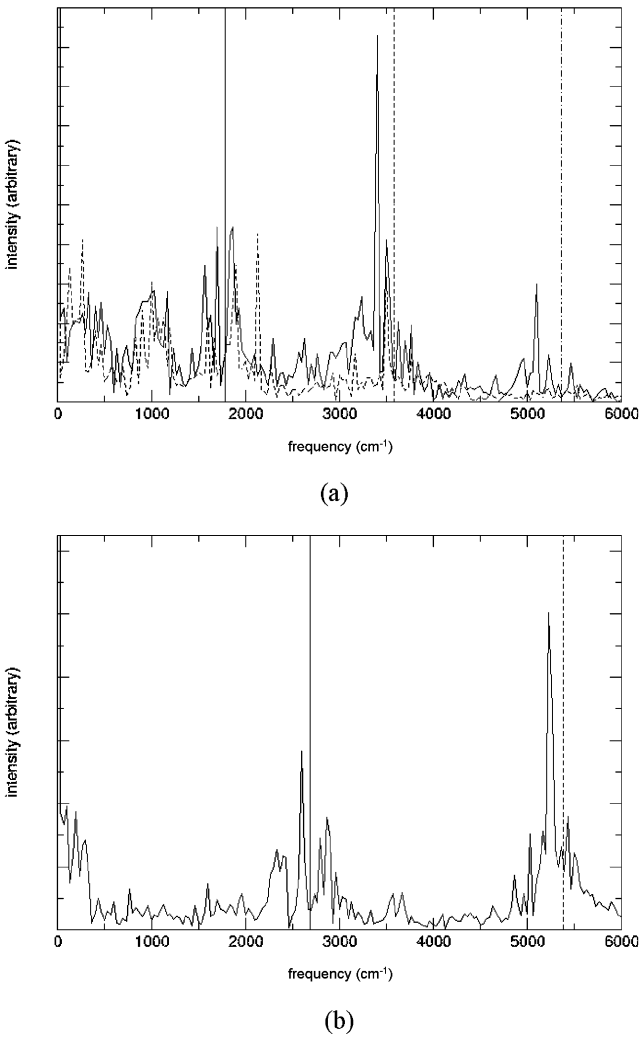


**Figure 3.** Power spectrum of the average velocity autocorrelation function for (a) each of the C−O bonds in the two formaldehyde molecules and (b) the •OH products formed from dissociation of •$CH_2OCH_2OOH$ through p-TS2 (see Figures 1 and 2). The solid-line black spectrum in part a is for the C−O bond in $CH_2$═O #1, and the dashed-line spectrum is for the C−O bond in $CH_2$═O #2. From left to right in both parts a and b, the solid vertical lines correspond to fundamental harmonic frequency according to DFT-B3LYP/6-31G** (1789 $cm^{-1}$ for the harmonic stretch of C−O and 2691 $cm^{-1}$ for the harmonic stretch of O−H(deuterated)). The vertical dashed lines mark the positions of the harmonic overtone frequencies, and the vertical -•- line represents the second harmonic overtone.

transition state, the C−O bonds in each fragment shorten. In contrast, fragment 1 (see Figure 2) is derived from an $sp^3$ hybridized carbon atom. Upon formation, this fragment is expected to have a lot of hydrogen wagging movement in and out of the plane and a little more C−O bond stretching than fragment 2, since its C−O bond shrinks from 1.323 to 1.207 Å, whereas the C−O bond of the terminal radical end $CH_2$═O moiety shrinks less, from 1.306 to 1.207 Å (according to DFT-B3LYP//6-31G** geometry optimization).

The power spectra of the average velocity autocorrelation function for the C−O bonds in the two product formaldehyde molecules appear in Figure 3a. These two spectra show clusters of peaks around the fundamental frequency (1789 $cm^{-1}$ according to DFT-B3LYP/6-31G**) and the first overtone (3578 $cm^{-1}$ of the C−O stretch in both $CH_2$═O molecules formed from p-TS2. For $CH_2$═O #1 (see Figure 2), another cluster of peaks appears close to the second overtone (5367 $cm^{-1}$). The red shift of the C−O overtone stretches are likely due to anharmonicity. The isotope effect of replacing the hydrogen with deuterium may not substantially influence our conclusions, since the difference between the C−O harmonic fundamental frequency of $CD_2$═O (1789 $cm^{-1}$) and $CH_2$═O (1847 $cm^{-1}$) is only 58 $cm^{-1}$, according to our DFT-B3LYP/6-31G** calculations. As discussed above, $CH_2$═O #1 has a longer initial C−O bond than that of $CH_2$═O #2, and this may contribute to the more intense C−O spectrum of $CH_2$═O #1 compared to that of $CH_2$═O #2, especially in the overtone region. Table 1 lists the vibrational, rotational, and translational energy breakdown of each fragment formed from the dissociation of p-TS2. From Table 1, the sum of the fragment energies shows that the $CH_2$═O #1 fragment has more internal energy on average than the $CH_2$═O #2 fragment. Thus, the excited C−O stretch evident in our simulations corroborates Maricq et al.'s explanation of the slow $CH_2$═O appearance in their real-time photolysis experiments. Though the C−O power spectrum alone indicates a possible vibrational excitation of the C−O bond, the C−O stretching contribution to the total power spectrum of the two formaldehyde fragments is very small (see Figure 4). The C−O stretching seems to couple strongly with the bending and stretching motion of the C−H bonds (hence the multiple peak clusters close to the harmonic fundamental and overtone modes of the C−O stretch). This may be more pronounced in $CH_2$═O #1, where the change in the hybridization of the carbon atom causes an out-of-plane wag. Thus, there may be a Fermi resonance mixing (and possibly Coriolis mixing) of the C−O stretch with the other modes of the formaldehyde that may also mask the C−O stretching mode from the tuned diode probe in the experiments of Maricq et al.

**TABLE 1: Estimated Breakdown of the Internal and Translational Energy Content (in kcal/mol) for the Two Formaldehyde and •OH Fragments from •$CH_2OCH_2OOH$ Dissociation (Averaged over 10 Trajectories)**

| energy type | $CH_2$═O #1 energy | $CH_2$═O #2 energy | •OH energy | total energy[a] |
|---|---|---|---|---|
| vibrational[b] | 20 ± 5 | 13 ± 5 | 4 ± 3 | |
| rotational[c] | 3 ± 1 | 4 ± 2 | 1 ± 1 | |
| translational[d] | 10 ± 2 | 7 ± 2 | 4 ± 3 | |
| total | 33 ± 5 | 24 ± 5 | 9 ± 3 | 66 ± 5 |

[a] The total system energy is defined as $E_{total} = E_{int}(CH_2{=}O\#1) + E_{int}(CH_2{=}O\#2) + E_{int}(OH) + E_{trans}(CH_2{=}O\#1) + E_{trans}(CH_2{=}O\#2) + E_{trans}(OH)$. $E_{int}$ for each fragment is the sum of the fragments' vibrational and rotational energies, and $E_{trans}$ is the fragment's translational energy. See the following footnotes for an explanation of how the vibrational, rotational, and translational energies were calculated. [b] Estimated by subtracting out the linear and angular momentum contributions to the total internal plus translational energy. [c] Estimated from the instantaneous rigid rotor approximation for each fragment (calculated from the angular momentum and its principal moments of inertia). [d] Estimated from center of mass motion of each fragment with respect to the center of mass of the total system.

The power spectrum of the O−H stretch of the •OH radical product is shown in Figure 3b. Interestingly, a peak at 5231 $cm^{-1}$ is close to the harmonic first overtone of the O−H (deuterium) stretch in •OH (deuterium) (5382 $cm^{-1}$). This is also red-shifted from the harmonic overtone peak, also due to anharmonicity. Thus, some of •OH radicals may have a vibrationally excited O−H stretch when produced from •$CH_2OCH_2OOH$ decomposition via p-TS2. This may have implications for quantitative measurement of •OH by laser-induced fluorescence (LIF).[62] In LIF, the $\tilde{A}\ ^2\Sigma^+ - \tilde{X}\ ^2\Pi$ electronic transition is commonly utilized for probing formation of •OH, and the ro-vibrational state of •OH is an important consideration.[62]

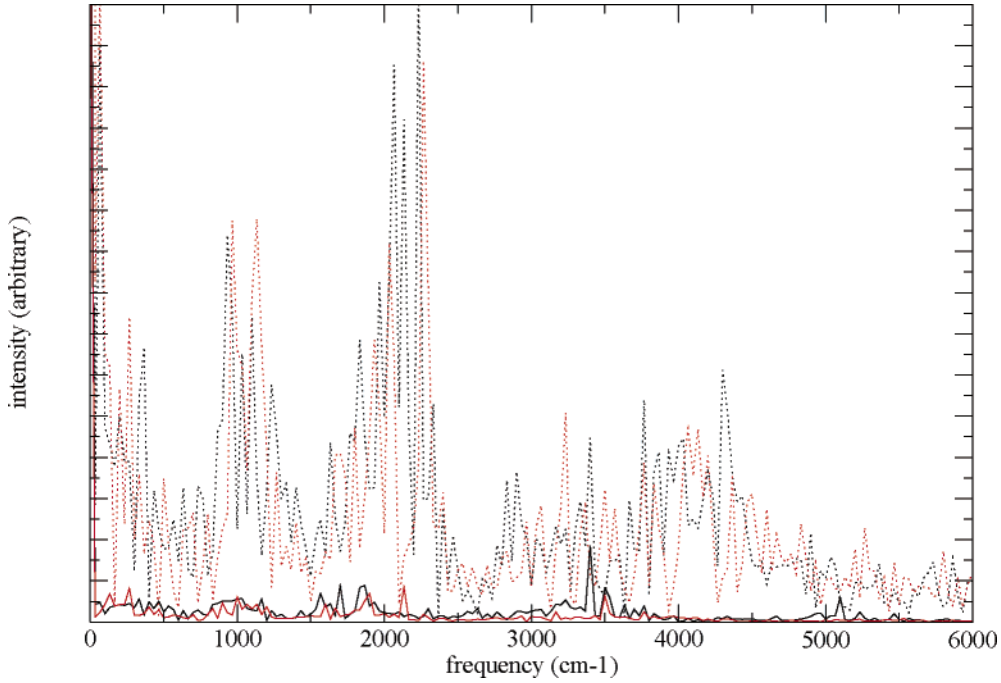


**Figure 4.** Comparison of the two formaldehyde molecule power spectra (black dotted line for $CH_2$═O #1 and red dotted line for $CH_2$═O #2) and their respective C−O power spectra (black solid line for C−O in $CH_2$═O #1 and red solid line for C−O in $CH_2$═O #2.

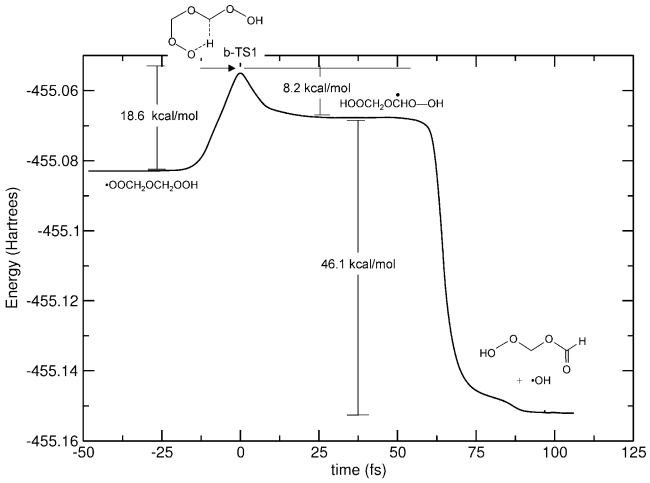


**Figure 5.** Damped dynamics plot (approximate IRC path) of the $HOOCH_2O\dot{C}HO-OH$ dissociation path to hydroperoxymethyl formate (HPMF) + •OH from b-TS1, within DFT-B3LYP//6-31G** theory. Note that the energies here are not zero-point-corrected.

**B. Trajectories from b-TS1 on the Way to Hydroperoxymethyl Formate.** Chain-branching begins with the addition of $O_2$ to $\bullet CH_2OCH_2OOH$ to form $\bullet O_2CH_2OCH_2OOH$. $\bullet OCH_2OCH_2OOH$ can dissociate back to $\bullet CH_2OCH_2OOH$ and $O_2$, or it can undergo hydrogen-transfer isomerization to form $HOOCH_2O\dot{C}HOOH$:

$$\bullet O_2CH_2OCH_2OOH \rightarrow HOOCH_2O\dot{C}HOOH \qquad (1)$$

The $HOOCH_2O\dot{C}HOOH$ is expected to be a very short-lived, metastable species. It undergoes dissociation via scission of the O−O bond to produce HPMF and •OH.

$$HOOCH_2O\dot{C}HO - OH \rightarrow HOOCH_2OC(=O)H + \bullet OH \qquad (2)$$

Reactions 1 and 2 are depicted in Figure 5 as a potential energy surface (PES) profile, according to our previous DFT-B3LYP damped-dynamics simulations.[5] Note that HPMF and •OH are expected to be formed with substantial excess energy because of the ∼46 kcal/mol drop to the HPMF + •OH well from $HOOCH_2O\dot{C}HOOH$'s "plateau" on the PES.

*1. Lifetime of $HOOCH_2O\dot{C}HOOH$.* The lack of a true minimum energy well on the potential surface for $HOOCH_2O\dot{C}HOOH$ suggests that it is a metastable intermediate of limited lifetime (see Figure 5). Thus, we set out to characterize exactly that. 70 trajectories were started from the deuterated b-TS1 transition state. In each case, we see a rapid migration of the transferring deuterium from the second carbon in $\bullet OOCH_2OCH_2OOH$ to the terminal oxygen (as expected from the PES generated with damped dynamics). Our dynamics show that the $HOOCH_2O\dot{C}HOOH$ is formed ∼8 fs into each trajectory. The lifetime of the $HOOCH_2O\dot{C}HOOH$ should be accessible with short-time dynamics, since its lifetime calculated from conventional transition state theory (CTST) is 216 fs at 600 K.[30] Our dynamics results more or less agree with this rough CTST estimate: $HOOCH_2O\dot{C}HOOH$ dissociates within 500 fs of its formation. Two of these 70 trajectories exhibited recrossing of this deuterium back to the original carbon site to recreate $\bullet OOCH_2OCH_2OOH$. Thus, there is a finite probability for recrossing the b-TS1 barrier. This is reasonable, since reaction 1 is endothermic by $\Delta H_0 = 14.9$ kcal/mol, according to our previous DFT-B3LYP calculations[5] ($\Delta E = 10.4$ kcal/mol, according to Figure 5). Moreover, the nascent $HOOCH_2O\dot{C}HOOH$ is only ∼8 kcal/mol below the b-TS1 transition state. Of course, such recrossing will produce deviations in kinetics predicted by CTST, which assumes no recrossing of the products over the transition state barrier to re-form reactants.

At first glance, it may be reasoned that this recrossing could be due to excess energy in the reaction coordinate. However, comparing the initial energies along the reaction coordinate of the trajectories involving recrossing with those that did not recross, we see that the "nonrecrossing" trajectories have initial reaction coordinate kinetic energies that are distributed above and below those of the trajectories exhibiting recrossing. Thus, initial reaction coordinate energy is not a likely contributor to recrossing. Instead, a more likely origin of recrossing is the

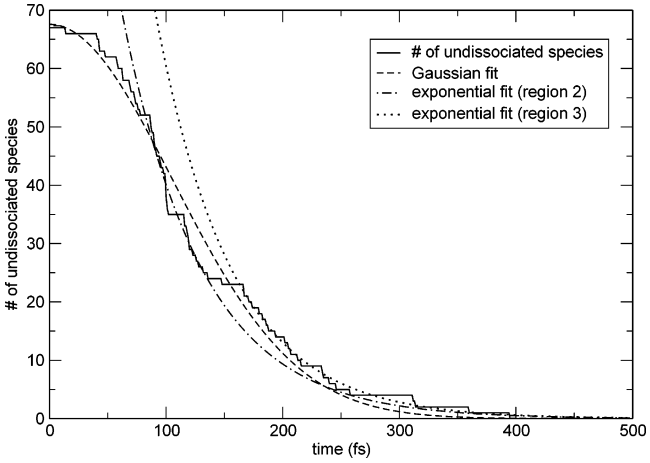


**Figure 6.** Number of trajectories (out of 68) where $HOOCH_2OCHO-OH$ has not dissociated to form HPMF + •OH vs time. The expected behavior for a random Poisson process would be exponential decay in time. The "Gaussian" has a width $\sigma = 105$ fs, which may be associated with an approximate lifetime of $HOOCH_2O\dot{C}HOOH$. Fits to the second (88−167 fs) and third (167−500 fs) sections (see text for details) are shown. The exponential fits for the second and third regions are $N_2(t) = 47.8 \exp[-1.46 \times 10^{-2}(t - 88)]$ and $N_3(t) = 21.6 \exp[-1.53 \times 10^{-2}(t - 167)]$, respectively.

rotation about the O−O bond upon H-transfer in $\bullet OOCH_2OCH_2OOH$ to form $HOOCH_2O\dot{C}HOOH$. If rotation around this bond is not rapid or sufficient enough, recrossing is most likely. Since the thermal selection of velocities favors excitation of low frequency modes, corresponding to the internal torsional motion, over high frequency bending and stretching modes, recrossing would be more prevalent at relatively low temperatures and less prevalent with increasing temperature. Thus, chain-branching reactions starting through reaction 1 could be inhibited initially because of some reversal of reaction 1 at relatively low temperatures (below 600 K). However, recrossing is slight at 600 K. As might be expected, coupling between the reaction coordinate and the stretching and bending degrees of freedom may be important in the recrossing process, but the torsional motion along the backbone destroys the favorable conformation for recrossing. Further work is needed to examine dynamics at temperatures above and below 600 K to validate the recrossing phenomenon.

With the remaining 68 successful trajectories (i.e., trajectories that involved dissociation of $HOOCH_2O\dot{C}HOOH$ into HPMF and •OH), the lifetime for $HOOCH_2O\dot{C}HOOH$ in each trajectory was used to generate a plot of the number of undissociated radicals vs time (in femtosecond). An exponential form was expected, where $N(t) = N_0 \exp(-t/\tau)$. Here $N(t)$ is the number of undissociated $HOOCH_2O\dot{C}HOOH$ radicals at a given time ($t$), $N_0$ is the initial number of $HOOCH_2O\dot{C}HOOH$ radicals, and $\tau$ is the lifetime (inverse of the rate).[63] Though many more trajectories than our humble 68 would be needed for an excellent statistical sampling, the plot of the number of dissociated $HOOCH_2O\dot{C}HOOH$ radicals vs time shown in Figure 6 has unexpected non-RRKM (i.e., nonergodic) behavior. Rather than following the expected ergodic exponential curve, the lifetime curve most closely fits a half-Gaussian-shape (with a correlation of 0.996). Microcanonical selection of the initial conditions was also tried to see if the Gaussian shape was an artifact of the canonical selection of initial conditions. Almost identical qualitative results were obtained with microcanonical initial conditions. RRKM theory is a microcanonical theory. However, convolution of microcanonical RRKM with a Boltzmann factor gives a canonical result, which will also be exponential in character if the unimolecular dynamics is ergodic.

RRKM theory[57,64,65] assumes that the internal energy distribution is random and complete, and the random lifetime distribution is expected to be of an exponential form $P(t) = k \exp(-kt)$ where $k$ is the rate of decay of an activated complex and $t$ is the time.[66] The time for energy transfer is assumed to be negligible compared to $1/k$.[66] The overall behavior illustrated in Figure 6 may appear to be Gaussian, but this curve can be viewed in three parts. The first part, the top of the "Gaussian" (0−88 fs), shows slow dissociation of the $HOOCH_2O\dot{C}HOOH$ radical, where only 28% have dissociated.

This observation of nonexponential behavior is indicative of "apparent" non-RRKM behavior due to chemical activation.[67,66] Slow IVR seen here can be likened to Rabinovitch and co-workers' classic example of apparent non-RRKM behavior: chemical activation to prepare vibrationally excited hexafluorobicyclopropyl-$d_2$, with subsequent decomposition via elimination of $CF_2$, where elimination of $CF_2$ is not immediate because chemical activation occurs on the opposite side of the molecule to where $CF_2$ is eliminated.[68] Upon formation, $HOOCH_2O\dot{C}HOOH$ has energy localized on the H-transfer side of the radical (the left side according to the chemical formula). Excess kinetic energy from $\bullet OOCH_2OCH_2OOH$ isomerization is expected to be pocketed in the newly formed H−O bond. This energy would take some nonnegligible amount of time to transfer along the H−O−O−C−O−Ċ−O−O−H backbone from the side with the newly formed H−O bond to the opposite side of the radical to hasten O−O scission. This could be why we see a nonexponential decrease in the number of nondissociated $HOOCH_2O\dot{C}HOOH$ with time. It is apparent from Figure 6 that the newly formed $HOOCH_2O\dot{C}HOOH$ does not dissociate immediately for the majority of trajectories. There appear to be a few trajectories with sufficient energy for O−O rupture in the first 88 fs of $HOOCH_2O\dot{C}HOOH$ formation. However, there is a dramatic decrease in the number of $HOOCH_2O\dot{C}HOOH$ radicals between 88 and 167 fs when a majority (41%) of the $HOOCH_2O\dot{C}HOOH$ is depleted. This second dissociation segment will be discussed next.

Another possible contribution to the nonergodic behavior seen in Figure 6 is the potential need for a proper $HOOCH_2O\dot{C}HOOH$ conformation that allows for O−O scission. Thus, the second segment, exhibiting a precipitous drop in surviving $HOOCH_2O\dot{C}HOOH$, may be due to "intrinsic" non-RRKM behavior of mode-specificity. This mechanism of mode specificity has been demonstrated extensively in the direct-dynamics simulations of Doubleday et al. for trimethylene isomerization, where trimethylene starts out in a shallow minimum with low barriers to isomerization.[38,37] Internal rotation and proper orbital orientation are important considerations in non-RRKM behavior of the systems studied by Doubleday et al.[37−39,69]

We observe in the molecular dynamics that the "ring" in b-TS1 must open up. That is, the first five heavy atoms of the HO−O−C−O−Ċ−O−OH backbone must rotate with respect to each other until the newly formed "HO" end is sufficiently far away from the Ċ radical center. Though this is not the only factor in $HOOCH_2O\dot{C}HOOH$ dissociation (the $HOOCH_2O\dot{C}HOOH$ that dissociate within the first 88 fs seem to have quite a bit of vibrational energy in the O−O bond or in deuterium wag of the adjacent radical carbon, which also disrupts the $\pi$-network), "unraveling" of the first five heavy centers of the b-TS1 ring seems to be a factor in the $HOOCH_2O\dot{C}HOOH$ lifetimes greater than 100 fs. Mode-specificity effects involving initial coupling to the reaction

**TABLE 2: Estimated Breakdown of the Internal and Translational Energy Content (in kcal/mol) for the HPMF and •OH Fragments from $HOOCH_2O\dot{C}HOOH$ Dissociation (Averaged over 68 Trajectories)**

| energy type | HPMF energy | •OH energy | total energy[a] |
|---|---|---|---|
| vibrational[b] | 53 ± 7 | 7 ± 4 | |
| rotational[c] | 5 ± 3 | 3 ± 2 | |
| translational[d] | 3 ± 1 | 18 ± 3 | |
| total | 61 ± 7 | 28 ± 4 | 89 ± 7 |

[a] The total system energy is defined as $E_{total} = E_{int}(HPMF) + E_{int}(OH) + E_{trans}(HPMF) + E_{trans}(OH)$. $E_{int}$ for each fragment is the sum of the fragment's vibrational and rotational energies, and $E_{trans}$ is the fragment's translational energy. See the following footnotes for an explanation of how the vibrational, rotational, and translational energies were calculated. [b] Estimated by subtracting out the linear and angular momentum contributions to the total internal plus translational energy. [c] Estimated from the instantaneous rigid rotor approximation for each fragment (calculated from the angular momentum and its principal moments of inertia). [d] Estimated from center of mass motion of each fragment with respect to the center of mass of the total system.

coordinate have led to biexponential behavior of the survival probability in the direct-dynamics simulations of Doubleday et al.[37,38] We may suspect the same of this second segment, but with a limited amount of data in this segment, we can only fit a single exponential (see Figure 6).

The final segment beyond 167 fs may involve trajectories (31%) where the $HOOCH_2O\dot{C}HOOH$ has lost memory of the initial configuration, and therefore may be more ergodic in dissociation. This final depletion of $HOOCH_2O\dot{C}HOOH$, gradually dropping off after 167 fs, has been fit to an exponential curve (see Figure 6).

*2. Energy distributions of HPMF and •OH.* Following the dissociation of $HOOCH_2O\dot{C}HOOH$, its dissociation products "fall" into a deep potential chasm. After crossing b-TS1, the products can gain a maximum of about 54 kcal/mol of excess internal (vibrational and rotational) and translational energy (on top of (hydrogenated) zero-point energy of 50 kcal/mol and thermal energy of ∼22 kcal/mol). However, the damped dynamics trajectory used to generate the PES in Figure 5 leads to a loosely bound $HOOCH_2OC(=O)H\cdots OH$ complex. About 5 kcal/mol is required to separate $HOOCH_2OC(=O)H$ and •OH. Thus, the maximum energy gain is actually ∼49 kcal/mol. With such an energy gain, it may be possible that HPMF gains a substantial amount of internal energy to react immediately via the many decomposition paths available to it (see Figure 1).

Upon decomposition, however, the •OH radical leaves with a fraction of this energy. An estimated breakdown of the vibrational, rotational, and translation energies imparted to both HPMF and •OH is listed in Table 2. HPMF apparently is formed with an estimated 61 kcal/mol internal and translational energy (including zero point and thermal energy). Most of this internal energy is vibrational energy (∼87%). There is some rotational energy (∼8%) and recoil translational energy (∼5%). Though rotational energy may aid in dissociation of HPMF, it is not as effective as internal vibrational energy for unimolecular decomposition of molecular systems.[57,64] The estimated vibrational energy of 53 kcal/mol in HPMF is only about 17 kcal/mol above the zero-point energy of deuterated HPMF (36.2 kcal/mol). The lowest barrier to HPMF unimolecular dissociation is through the formation of a hydrogen-bonded $HC(=O)OH\cdots CH_2OO$ complex, which is about 32 kcal/mol above the energy for HPMF (30 kcal/mol when zero-point energy is considered); another 12 kcal/mol is needed to fully dissociate the loose

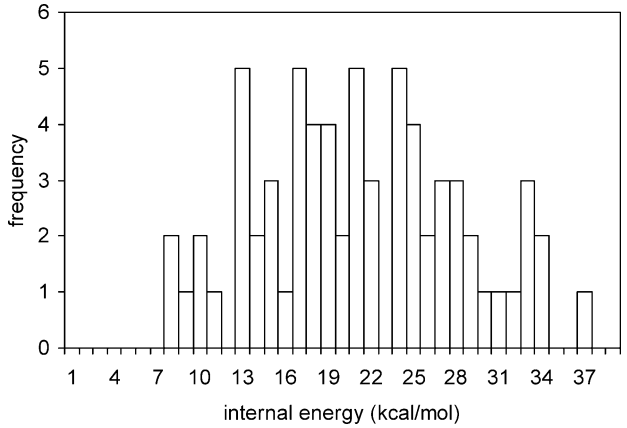


**Figure 7.** Histogram depicting the HPMF internal energy (vibrational + rotational minus the zero-point energy) distribution upon the dissociation of $HOOCH_2O\dot{C}HO-OH$ to form HPMF and •OH.

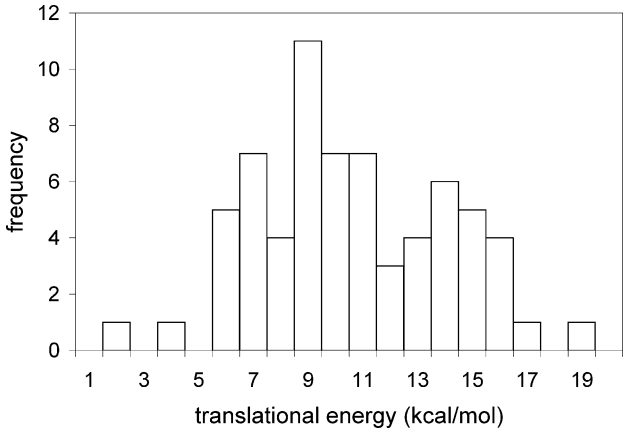


**Figure 8.** Histogram depicting the •OH translational energy distribution upon the dissociation of $HOOCH_2O\dot{C}HO-OH$ to form HPMF (deuterated) and •OH. Note the possible trimodal character of the distribution.

$HC(=O)OH\cdots CH_2OO$ complex to $HC(=O)OH$ and $CH_2OO$. Only 13% of the HPMF molecules formed in our simulations have sufficient internal energy (above the zero-point energy) to surmount this barrier. The mean internal energy (above the zero-point energy) of the HPMF is 22 kcal/mol with a standard deviation of 7 kcal/mol (see Figure 7 to view the distribution of energies). Thus, most HPMF may not have enough energy to undergo unimolecular dissociation upon formation and may require activation via collisions to decompose. Unfortunately, the number of degrees of freedom for HPMF along with the inclusion of a model to simulate collisions (either implicitly or explicitly) makes direct DFT-B3LYP BOMD of the HPMF decomposition process computationally prohibitive.

•OH contains an estimated 31% of the internal and translational energies of the HPMF and •OH. Unlike HPMF, most of this energy is in translational motion (about 64%). This translational energy accounts for about 20% of the total energy (see Table 2). The distribution of •OH translational energy appears in Figure 8. There is a small negative correlation between the lifetime of $HOOCH_2O\dot{C}HOOH$ and the translational energy of •OH (correlation coefficient of −0.3), which is expected since translational motion of •OH occurs along the reaction coordinate to $HOOCH_2O\dot{C}HOOH$ dissociation. Thus, the possible trimodality seen in Figure 8 may be related to the three-stage behavior seen in the lifetime curve in Figure 6. The early time decay into HPMF + •OH may be associated with the fast (high kinetic energy) •OH component of Figure 8.

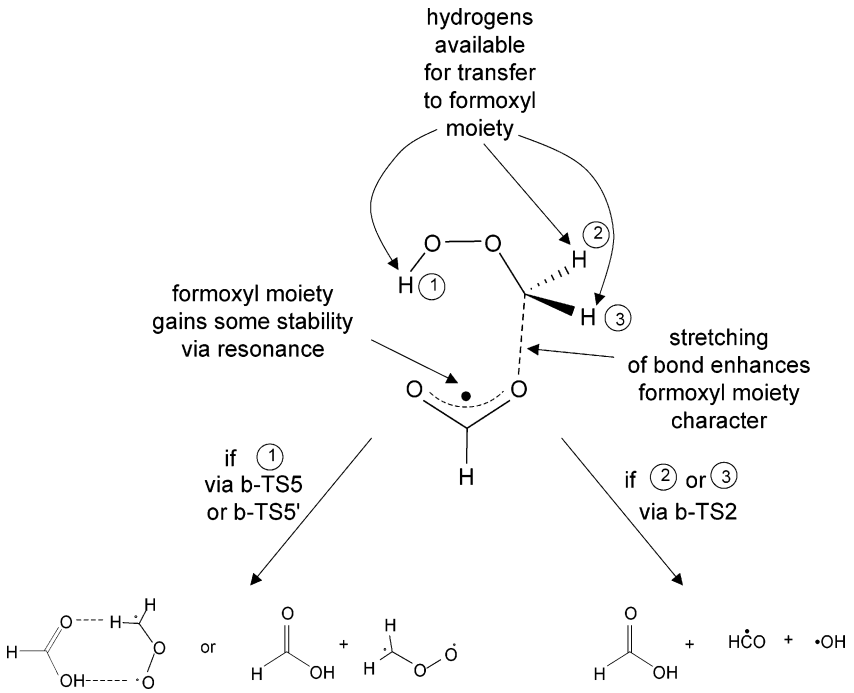


**Figure 9.** Scheme depicting the reason barriers to reaction involving the b-TS2, b-TS5, and b-TS5′ transition states are the lowest tight transition states and why formation of a hydrogen-bonded formic acid/Criegee intermediate complex is favorable.

However, the origin of the later time decay components of Figure 6 is unclear. The bending and stretching motions of the −CHOOH end may dissipate its vibrational energy into the rest of the radical system, resulting in a more ergodic distribution of those $HOOCH_2O\dot{C}HOOH$ that decay at later times.

About 25% of the energy imparted to •OH is vibrational (Table 2). The ∼7 kcal/mol of vibrational energy is ∼3 kcal/mol higher than zero-point energy. However, not all trajectories conserve zero-point energy (35% had vibrational energies below 3.8 kcal/mol). The zero-point leakage problem is a well-known problem with the classical propagation of the nuclei,[70,71] and techniques have been proposed to treat this problem.[71,72,73,74] Using the Einstein−Keller−Brillouin (EKB) binning,[54] we find that about 47% of the •OH can be assigned to the $v = 1$ state, while one out of the 68 trajectories has an •OH in $v = 2$. Thus, 49% (almost half) of the •OH created from $HOOCH_2O\dot{C}HOOH$ is vibrationally excited, which is an important consideration for quantitative determination of •OH from LIF probing of the $\tilde{A}\ ^2\Sigma^+ - \tilde{X}\ ^2\Pi$ electronic transition.[62] Again, these likely correspond to the slower moving •OH radicals formed.

**C. HPMF Decomposition.** According to our conventional transition state theory results, the HPMF decomposition path with the lowest barrier to reaction (HPMF to $CH_2OO\cdots HC(=O)OH$) has a lower bound to the HPMF decomposition time at 600 K of 0.2 ms.[30] Thus, HPMF (deuterated) created in the course of the BOMD simulations started from b-TS1 (in section 3.2) is not expected to decompose in the short time constraints of BOMD (typically picoseconds). So instead we start trajectories from the saddle-point structures b-TS2, b-TS5, and b-TS5′ leading to HPMF decomposition into $HC(=O)OH + H\dot{C}O$ + •OH, $CH_2OO$ + HC(=O)OH, and $CH_2OO\cdots HC(=O)OH$, respectively. These are the lowest tight (i.e., having a true first-order saddle-point structure) barriers to HPMF decomposition. Unfortunately, we cannot model O−O scission because this reaction is apparently "barrierless" (i.e., having no true saddle-point structure). Forsythe et al. have developed ab initio molecular dynamics techniques for proper setup of the dividing surface for reactions involving loose transition states, which may be promising for future simulations of O−O scission in HPMF.[75]

Figure 9 illustrates similarities in the concerted reactions involving HPMF via the b-TS2, b-TS5, and b-TS5′ transition states. From the damped dynamics calculations done in previous work,[5] we see a lengthening of the C−O bond followed by H-transfer through b-TS2, b-TS5, and along the path leading to $CH_2OO\cdots HC(=O)OH$ via b-TS5′. The lengthened C−O bond is favorable, since a partial resonance-stabilized formoxyl radical is made possible by this lengthening (as illustrated in Figure 9). The driving force for H-transfer to the formoxyl moiety is large since formic acid ($\Delta H_f^\circ(298K) = -90.5$ kcal/mol[76,77]) is much more thermodynamically stable than formoxyl radical ($\Delta H_f^\circ(298\ K) = -35.5$ kcal/mol[78]).

*1. HPMF Decomposition from b-TS2, b-TS5, and b-TS5′.* HPMF decomposition reactions are all endothermic (Figure 1), with product-like transition states in accord with Hammond's postulate. The forward path from b-TS2 (to products) shows that the C−O bond lengthens, followed by transfer of a hydrogen from the $-CH_2-$ section of HPMF. This reaction is endothermic by 39.0 kcal/mol ($\Delta H_{rxn}$(298 K), DFT-B3LYP//6-31G**).[5] Like b-TS2, b-TS5 is product-like. The endothermicity of HPMF decomposition to $CH_2OO$ and HC(=O)OH through b-TS5 is 44.3 kcal/mol ($\Delta H_{rxn}$(298 K), DFT-B3LYP//6-31G**).[5] Note that although b-TS2 is a higher barrier to reaction than b-TS5′, b-TS2 is more favorable entropically ($\Delta S^\ddagger(298\ K) = 9.2$ cal/mol·K) than b-TS5′ ($\Delta S^\ddagger(298\ K) = 5.7$ cal/mol·K) and b-TS5 ($\Delta S^\ddagger(298\ K) = 5.7$ cal/mol·K) because b-TS2 directly leads to three products: $H\dot{C}O$, •OH, and HC(=O)OH. Though the b-TS2 barrier is more entropically favorable than that for b-TS5 and b-TS5′, the free energy for b-TS2 ($\Delta G^\ddagger(298\ K) = 42.5$ kcal/mol) is only slightly lower than that of b-TS5 ($\Delta G^\ddagger(298\ K) = 43.1$ kcal/mol) and much higher than that of b-TS5′ ($\Delta G^\ddagger(298\ K) = 28.8$ kcal/mol). Thus, the b-TS5′ $CH_2OO\cdots HC(=O)OH$ would still be the more kinetically favorable product (note that ∼12 kcal/mol is still needed to fully dissociate the $CH_2OO\cdots HC(=O)OH$ complex to $CH_2OO$ and HC(=O)-

OH). The kinetics of HPMF decomposition via b-TS2 is only slightly more favorable than the HPMF decomposition via b-TS5.

Ten trajectories from b-TS5 and ten trajectories from b-TS5′ were run in the forward direction toward the HPMF decomposition products $CH_2OO$ + HC(=O)OH and $CH_2OO\cdots$HC(=O)OH, respectively. These trajectories only yielded $CH_2OO$ and HC(=O)OH products. At 600 K, the less stable product, $CH_2OO$, would need at least 3.8 $\mu$s to react to form dioxirane (c-$CH_2OO$), according to our conventional transition state theory calculations.[30] Simulation temperatures well over 2000 K would be needed to see any reaction of the $CH_2OO$ product within 2−3 ps. With extremely low exit channel barriers to $CH_2OO$ + HC(=O)OH, some of the trajectories from b-TS5 and b-TS5′ propagated toward the products recrossed their respective barrier to re-form HPMF. By contrast, trajectories starting from b-TS2 toward dissociation products showed more interesting behavior that will be discussed next.

In our trajectories started from b-TS2, a van der Waals cluster of HC(=O)OH and the HĊOOH (HC(=O)OH$\cdots$HĊOOH) forms initially. With a fairly small barrier to HPMF formation from the product side (~7 kcal/mol at the DFT-B3LYP/6-31G** level of theory[5]), we observed six of our 30 trajectories from b-TS2 toward products recrossed b-TS2 and re-formed HPMF:

$$\text{HC(=O)OH}\cdots\text{HĊOOH} \rightarrow \text{HOOCH}_2\text{OC(=O)H} \quad (3)$$

When re-formation of HPMF does not occur, the formic acid and HĊOOH metastable radical do not readily separate. Then, 10 of the 30 trajectories yield fully formed HĊO, •OH, and HC(=O)OH.

$$\text{HC(=O)OH}\cdots\text{HĊOOH} \rightarrow \text{HĊO} + {}^{\bullet}\text{OH} + \text{HC(=O)OH} \quad (4)$$

However, another 10 of the 30 trajectories unexpectedly show the HC(=O)OH$\cdots$HĊOOH complex rearranging to form formic acid anhydride (HC(=O)OC(=O)H; FAA) and $H_2O$:

$$\text{HC(=O)OH}\cdots\text{HĊOOH} \rightarrow \text{HC(=O)OC(=O)H} + \text{H}_2\text{O} \quad (5)$$

Snapshots of a representative trajectory showing the rearrangement of HĊOOH to $H_2O$ + FAA are shown in Figure 10. The snapshot at 230 fs shows that the nascent •OH formed from the short-lived HĊOOH complex is close enough to attack the deuterium of the nascent formic acid molecule to form $H_2O$. This water molecule is formed vibrationally excited (there is little to no barrier for this deuterium abstraction). This is not the first time that the high reactivity of •OH has been demonstrated in molecular dynamics simulations. Frank et al.[79] have shown in their DFT-B3LYP MD simulations of •OH reacting with 3-hexanone that the •OH, having a highly electrophilic character, readily forms H-bonded complexes and van der Waals adducts, which eventually can lead to formation of highly vibrationally excited $H_2O$.

The remaining formoxyl and HĊO fragments are in close enough proximity to combine to form FAA (see 300 fs snapshot of Figure 10). This is a fairly long-ranged attraction since both formoxyl and HĊO are radical species. Thus, their recombination is barrierless and the resulting FAA is highly vibrationally excited (as with the $H_2O$). The drive to form $H_2O$ and FAA can also be partly but not entirely (since the system is not at equilibrium) explained with thermodynamics. Figure 11 shows a detailed illustration of the paths leading to HPMF decomposition including an HPMF decomposition path leading to $H_2O$ and FAA. The path leading to $H_2O$ + FAA has a barrier higher than those of the paths considered in Figure 1. Thus, it was not considered to be a viable path for HPMF decomposition. However, compared with the products from paths with lower barriers, the $H_2O$ and FAA products are much more thermodynamically favorable than the other HPMF decomposition products from more kinetically favorable paths. Unlike other pathways, the decomposition of HPMF to $H_2O$ + formic acid anhydride is an exothermic reaction: −52.7 kcal/mol at the DFT-B3LYP//6-31G** level of theory.[28,5] We see from our molecular dynamics that the simple picture of direct formation of FAA being disfavored kinetically is not relevant once dynamics is taken into account; subsequent rearrangements after going through the kinetically favored paths allow its formation to occur. FAA and $H_2O$ are known to be common decomposition products of HPMF under atmospheric conditions.[26] Under diesel engine conditions, however, we expect numerous collisions to occur with the molecules present in the engine. Unfortunately, we cannot easily incorporate collisions of the possible molecules that HPMF could encounter because of the computational expense. It is expected that HPMF's highly reactive radical products would easily react with many of the combustion species they collide with (including dimethyl ether itself), thereby somewhat limiting production of FAA.

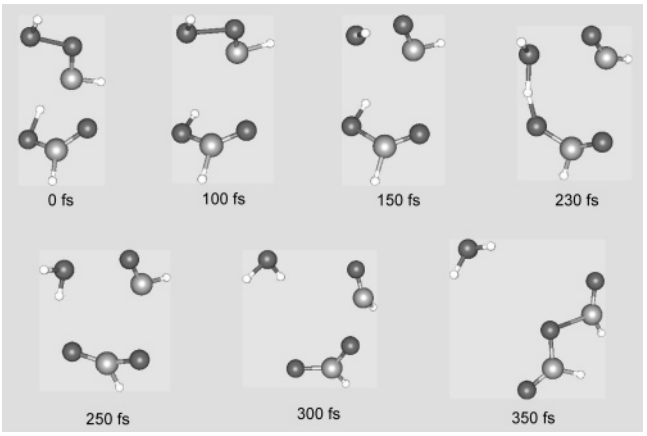


**Figure 10.** Snapshots of the rearrangement of the initial HC(=O)OH + HĊO + •OH products to form $H_2O$ + HC(=O)OC(=O)H (formic acid anhydride). The dark gray balls are oxygens, the light gray balls are carbons, and the white balls are deuteriums. $t$ = 0 fs corresponds to the b-TS2 transition state. Note that at 150 fs, the initial products are HC(=O)OH + HĊO + •OH. At 230 fs, the •OH fragment removes the hydroxyl deuterium from HC(=O)OH to form $H_2O$ and a formoxyl radical. At 300 fs, the HĊO approaches the formoxyl radical, and, at 350 fs we see that the HĊO and formoxyl radical have formed formic acid anhydride (FAA, HC(=O)OC(=O)H).

Rather than producing FAA after •OH removes the hydroxyl deuterium from the nascent HC(=O)OH to form $H_2O$ and formoxyl radical (as in Figure 10), the HĊO radical also can lose its deuterium to the formoxyl radical to produce CO and a new HC(=O)OH:

$$\text{HC(=O)OH}\cdots\text{HĊOOH} \rightarrow \text{CO} + \text{H}_2\text{O} + \text{HC(=O)OH} \quad (6)$$

This occurs in two of the 30 trajectories. Snapshots of one of the trajectories are shown in Figure 12. At 165 fs, the nascent •OH radical abstracts the hydroxyl deuterium from the HC(=O)OH fragment. In the snapshot at 280 fs, the deuterium of the nascent HĊO is transferred to the formoxyl radical. The oxygen of the newly formed $H_2O$ is close to this deuterium and appears to be aiding the deuterium transfer process. $H_2O$, CO, and

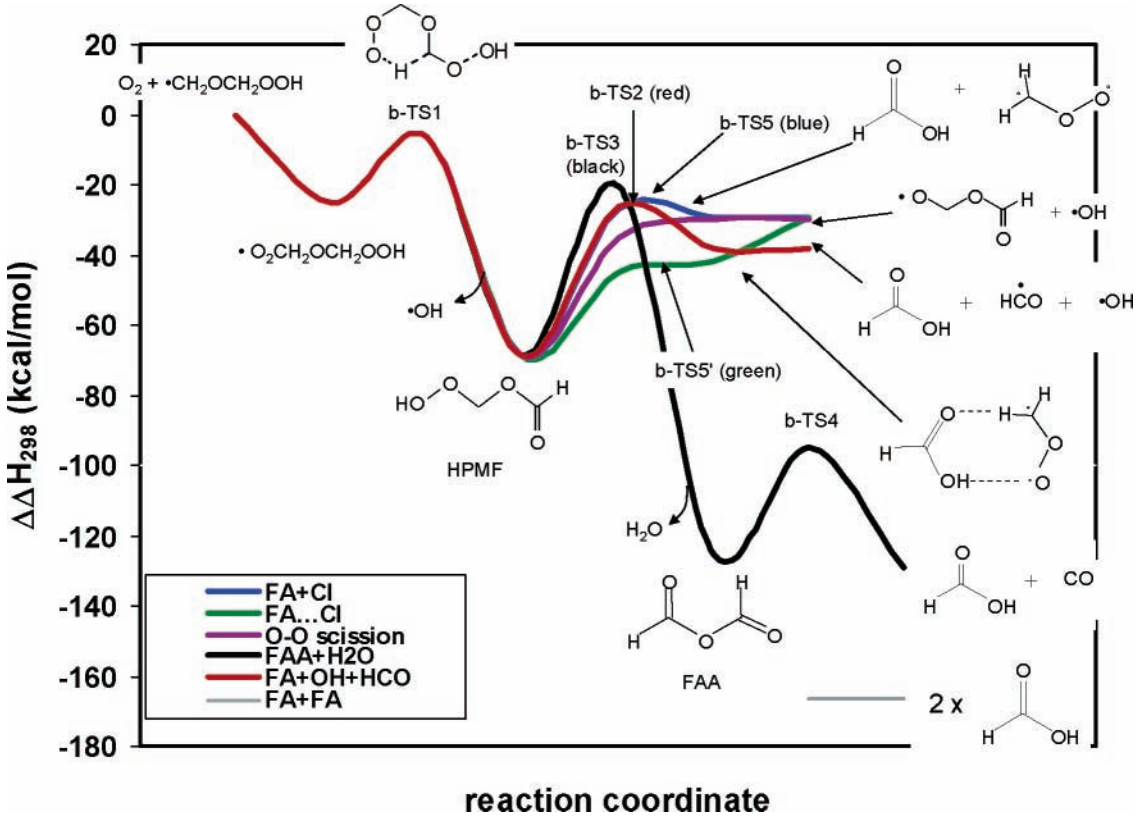


**Figure 11.** Potential energy surfaces of HPMF decomposition along the chain-branching path. Note the high thermodynamic stability of the formation of $H_2O$ and formic acid anhydride (FAA, HC(=O)OC(=O)H). "FA" and "CI" stand for formic acid (HC(=O)OH) and $CH_2OO$ (Criegee intermediate), respectively.

HC(=O)OH are much more stable products than •OH, HĊO, and HC(=O)OH: $\Delta H_f(298\ K) = -174.7$ kcal/mol for the former group of hydrogenated species[76,77,80] vs $\Delta H_f(298\ K) = -70.8$ kcal/mol for the latter group of hydrogenated species[76,77,80]. One trajectory leads to the creation of two rather than one HC(=O)OH:

$$HC(=O)OH\cdots H\dot{C}OOH \rightarrow HC(=O)OH + HC(=O)OH \quad (7)$$

Selected snapshots for this trajectory are shown in Figure 13. The trajectory starts off on the same course as the trajectories leading to FAA + $H_2O$ and $H_2O$ + CO + HC(=O)OH, with the nascent •OH heading toward abstraction of the hydroxyl deuterium of the newly formed formic acid molecule. However, the HĊO is still in close proximity to the •OH radical as it makes its way toward the hydroxyl deuterium. When •OH attacks this hydroxyl deuterium, the radical carbon of HĊO latches on to the •OH and forms a new HC(=O)OH (see the snapshot at 630 fs in Figure 13). In this trajectory, it seems that HC(=O)OH aids in rearranging HĊOOH to produce a second formic acid. As with the previous two cases described above, the formation of two HC(=O)OH is more thermodynamically probable (−181.0 kcal/mol[76,77]) than the formation of •OH, HĊO, and HC(=O)OH (−70.8 kcal/mol[76,77,80]).

The rearrangement of •OH, HĊO, and HC(=O)OH to form FAA and $H_2O$ was not the only unexpected outcome seen in our 30 trajectories from b-TS2. One of the 30 trajectories underwent rearrangement of the HĊOOH and HC(=O)OH fragments to form the Criegee intermediate $CH_2OO$ and HC(=O)OH:

$$HC(=O)OH\cdots H\dot{C}OOH \rightarrow CH_2OO + HC(=O)OH \quad (8)$$

Snapshots from a representative trajectory showing the rearrangement of HĊOOH and HC(=O)OH to form $CH_2OO$ and HC(=O)OH are shown in Figure 14. In this case, the HĊOOH does not fully dissociate to form HĊO and •OH as seen in the previous case of FAA + $H_2O$ production (Figure 10). Instead, a "lining-up" of both the radical orbital of HĊOOH with the hydroxyl deuterium of HC(=O)OH and of the hydroxyl deuterium of the HĊOOH with the carbonyl oxygen of the HC(=O)OH occurs in the first few hundred femtosecond. A failed attempt of transferring the HC(=O)OH hydroxyl deuterium occurs at 320 fs. A second attempt at this deuterium transfer occurs around 500−515 fs, which is successful. The transfer of the hydroxyl deuterium of the HC(=O)OH to HĊOOH at 515 fs is promptly followed by a transfer of the hydroxyl deuterium of HĊOOH to the carbonyl oxygen of HC(=O)OH at 530 fs. By 600 fs, there are discernible $CH_2OO$ and HC(=O)OH fragments. The lowest lying path of HPMF dissociation involves the formation of $CH_2OO\cdots$HC(=O)OH complex through b-TS5′ (see Figure 11). This path involves a transfer of the peroxide hydrogen on HPMF to the carbonyl oxygen on the other side of the HPMF molecule along with a C−O stretch, as depicted in Figure 9. This path leads to a product, ($CH_2OO\cdots$HC(=O)OH), that is lower in energy than the •OH, HĊO, and HC(=O)OH produced through b-TS2. Thus, the formation of $CH_2OO\cdots$HC(=O)OH, like FAA + $H_2O$, is both a thermodynamically and kinetically favorable outcome.

To further explore the kinetics and thermodynamics of the products observed in these simulations starting from b-TS2, we have have listed the $\Delta G$, $K_{eq}$, branching ratios calculated from $K_{eq}$ and from the MD trajectories for all reactions starting from b-TS2 in Table 3. From the equilibrium constants and their respective branching ratios, it can be argued that the most likely reaction to take place is reaction 6, closely followed by reaction

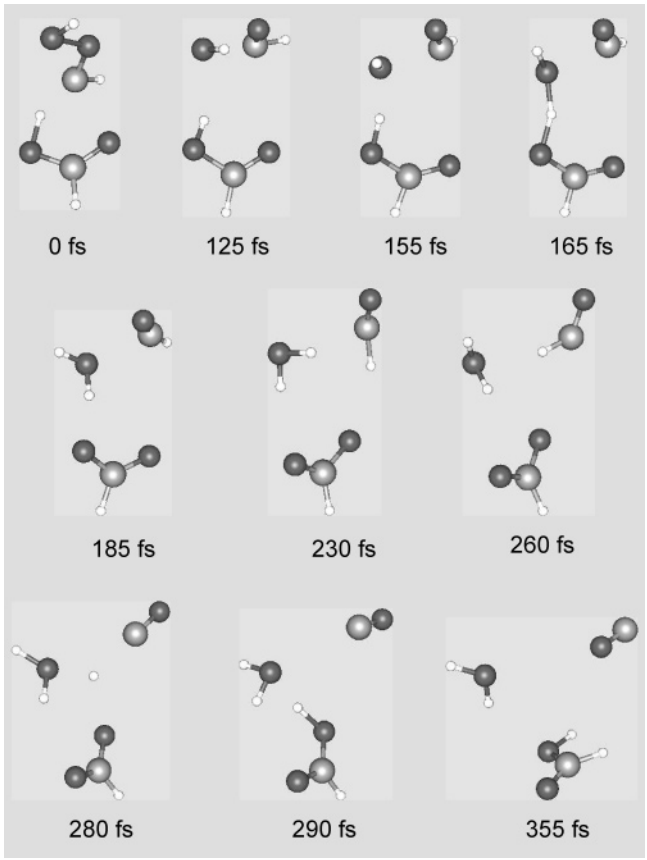


**Figure 12.** Snapshots of the rearrangement of HC(═O)OH + HĊO + •OH to form CO + $H_2O$ + HC(═O)OH. $t = 0$ fs corresponds to the b-TS2 transition state. At 155 fs, the HĊOOH fragment dissociates to HĊO and •OH. At 165 fs, the •OH abstracts the hydroxyl deuterium from HC(═O)OH to form $H_2O$ and formoxyl radical. At 280 fs, the deuterium of HĊO is abstracted by the formoxyl radical to form CO and HC(═O)OH.

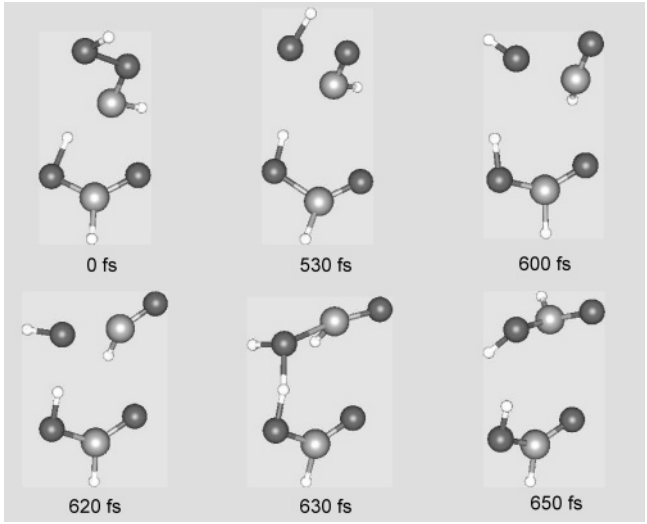


**Figure 13.** Snapshots of the rearrangement of the HC(═O)OH + HĊO + •OH to form two HC(═O)OH. $t = 0$ fs corresponds to the b-TS2 transition state. At 530 fs, the HĊOOH fragment dissociates to HĊO + •OH. At 620 fs, the •OH is observed approaching the hydroxyl deuterium of HC(═O)OH, and, at 630 fs, the •OH makes an attempt at abstracting this hydroxyl deuterium of HC(═O)OH. At 650 fs, the •OH has failed to abstract the hydroxyl deuterium of HC(═O)OH and has been captured by the HĊO to form a second HC(═O)OH.

7. The much less likely reactions are reactions 4, 5, and 8, with reaction 8 being the least stable thermodynamically. By contrast,

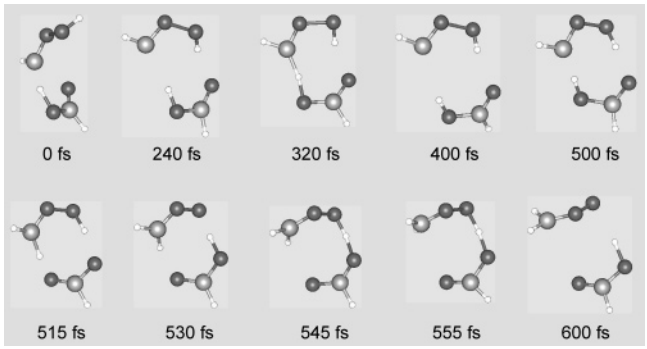


**Figure 14.** Snapshots of the rearrangement of the HC(═O)OH + HĊO + •OH to form $CH_2OO$ + HC(═O)OH. $t = 0$ fs corresponds to the b-TS2 transition state. At 320 fs, the HĊOOH makes an attempt to abstract the hydroxyl deuterium from the HC(═O)OH. This abstraction attempt failure is shown at 400 fs. At 500 fs, the HC(═O)OH and HĊOOH approach each other again. At 515 fs, HĊOOH abstracts the hydroxyl deuterium of HC(═O)OH. At 530 fs, the formoxyl created in this abstraction attempts to abstract the peroxide deuterium of the nascent •$CH_2OOH$. At 545 and 555 fs, the •$CH_2O$− group of •$CH_2$-OOH appears to be rotating so that the 2p orbital containing the radical electron is pointed toward the formoxyl. At 600 fs, abstraction of •-$CH_2OOH$'s peroxide deuterium by the formoxyl to form HC(═O)OH and $CH_2OO$ is complete.

branching ratios from the dynamics show that reaction 4 and reaction 5 have the most dominant products from b-TS2. The products of reaction 4 are thus clearly kinetically controlled products, but the products of reaction 5 appear equally likely, suggesting that their favorable thermochemistry plays an important role in their appearance. Reactions 5−7 are the most thermodynamically favorable. However, these products are the result of multiple steps after b-TS2, and, therefore, are likely to not be kinetically favorable. This could explain the relatively low branching ratios of the products of reactions 6 and 7.

So, 30 trajectories is too limited of a sampling for gathering statistics on the myriad of products that may be observed in our trajectories from b-TS2. Though the path through b-TS2 is not the most favorable path to HPMF decomposition (see Figure 11), the trajectories ran from b-TS2 do show us that the many paths to decomposition of this highly oxygenated compound are interconnected. Since all paths to HPMF decomposition are interconnected from a dynamics point-of-view, this is bound to have an effect on the underlying kinetics, namely that the low-temperature chain branching kinetics of DME is more complex than once thought.[3,33,30]

## IV. Summary and Conclusions

We present Born−Oppenheimer molecular dynamics (BOMD) simulations for selected portions of the deuterated DME chain propagation and chain branching potential energy surfaces. Although our notation throughout refers to "H" rather than "D" for simplicity, the dynamics were all performed on deuterated species to justify the classical treatment of nuclei in the BOMD method. Thus, our calculations will underestimate the reaction dynamics/kinetics whenever tunneling may be important. Nevertheless, our short-time dynamics reveal complex, intriguing behavior not predicted by conventional statistical rate theories (e.g., CTST and RRKM). We studied three areas of the chain propagation and branching PESs where short-time dynamics had the prospect of showing interesting phenomena. The first of these regions was along the chain propagation pathway for DME oxidation, involving the dissociation of •$CH_2OCH_2OOH$ to form two $CH_2$═O and •OH. Trajectories were started at p-TS2 (the transition state for dissociation of •$CH_2OCH_2OOH$) in the

**TABLE 3: The Free Energy Change, the Equilibrium Constant, and the Number of Trajectories Representing the Outcome of Each Respective Competing b-TS2 Reaction (at the DFT-B3LYP/6-31G** Level of Theory with Deuterated Species)[a]**

| reaction | corresponding equation[b] | $\Delta G$ (kcal/mol) | $K_{eq}$ | branching ratio from $K_{eq}$ | branching ratio from simulations |
|---|---|---|---|---|---|
| HPMF → HĊO + •OH + HC(═O)OH | 4 | −4.5 | $4.42 \times 10^{1}$ | $1.1 \times 10^{-33}$ | 0.42 |
| HPMF → HC(═O)OC(═O)H + $H_2O$ | 5 | −75.9 | $4.51 \times 10^{27}$ | $1.1 \times 10^{-7}$ | 0.42 |
| HPMF → CO + $H_2O$ + HC(═O)OH | 6 | −94.9 | $3.63 \times 10^{34}$ | 0.89 | 0.08 |
| HPMF → HC(═O)OH + HC(═O)OH | 7 | −92.4 | $4.62 \times 10^{33}$ | 0.11 | 0.04 |
| HPMF → $CH_2OO$ + HC(═O)OH | 8 | 20.3 | $4.04 \times 10^{-8}$ | $9.9 \times 10^{-43}$ | 0.04 |

[a] The temperature and pressure for these calculations were 600 K and 1 atm, respectively. [b] As enumerated in the text.

forward direction toward the products, two $CH_2$═O and •OH. Maricq et al.[32] reported that the rate of $CH_2$═O formation in their real-time laser photolysis experiments was slow compared to the rate derived by Sehested et al.[31] using indirect smog chamber techniques. They attributed this slow rate of $CH_2$═O formation to excited C−O stretching in the nascent $CH_2$═O, which would be invisible to the diode laser probing the $\nu = 0 \rightarrow 1$ C−O stretch transition. The power spectra of the average C−O and O−H velocity correlation functions constructed by us shows that the C−O stretch of formaldehyde exhibits first and second (clustered) overtone peaks, which lends credence to Maricq et al.'s[32] proposal that the excited C−O formaldehyde stretch is the source of apparent slow formaldehyde appearance. Moreover, the C−O stretch appears to be strongly coupled to the other bending and stretching vibrational modes, which involve C−H bonds. This may be a possible reason for the initial invisibility of the formaldehyde to the diode laser probe in the experiments of Maricq et al. The •OH radical may be formed vibrationally excited as well.

Simulations started in the forward direction from b-TS1, the isomerization transition state from •$OOCH_2OCH_2OOH$ to $HOOCH_2O\dot{C}HOOH$ along the DME chain-branching path, show that a small number of trajectories (2 out of 70, or 3%) recross the b-TS1 barrier. This recrossing is to be expected, since the formation of the short-lived metastable radical $HOOCH_2O\dot{C}HOOH$ from •$OOCH_2OCH_2OOH$ is very endothermic and the barrier to recrossing b-TS1 to re-form •$OOCH_2OCH_2OOH$ is only ∼8 kcal/mol (see Figure 5). This shows that HPMF + •OH formation along the chain branching path may be inhibited by recrossing to re-form •$OOCH_2OCH_2OOH$. Since low-frequency torsional modes important along the reaction path are weighted more in the thermal momentum and coordinate displacement selection than high-frequency bending and stretching modes, we would expect to see an increase in recrossing at temperatures lower than 600 K, because the torsion of the nascent OH group seems to be the dominant factor in inhibiting recrossing to re-form •$OOCH_2OCH_2OOH$.

For the remaining 68 trajectories where recrossing does not occur, the lifetime of $HOOCH_2O\dot{C}HOOH$ does not demonstrate an ergodic (RRKM) pattern of dissociation to HPMF and •OH. The survival probability instead follows a Gaussian-like falloff. However, the behavior of the $HOOCH_2O\dot{C}HOOH$ lifetime can be understood by dividing the plot into three regions. The first region (0−88 fs) may be indicative of "apparent" non-RRKM behavior via chemical activation. Upon formation of $HOOCH_2O\dot{C}HOOH$ via b-TS1, the nascent H−O in which most of the newly gained 8 kcal/mol is expected to be located is on the opposite side of the radical from where O−O dissociation will occur. Therefore, it is expected that this energy is slow to dissipate throughout the radical to allow for ergodic dissociation of $HOOCH_2O\dot{C}HOOH$ to HPMF and •OH. However, an "intrinsic" non-RRKM process may also occur, which could explain the sharp decline in surviving $HOOCH_2O\dot{C}HOOH$ molecules in the 88−167 fs region. The right orientation may need to be achieved by torsional motion of the H−O−O−C−O−C−O−O−H backbone to allow for dissociation of the short-lived $HOOCH_2O\dot{C}HOOH$ complex. More ergodic behavior is observed after 167 fs as the internal energy becomes more randomly distributed in the remaining $HOOCH_2O\dot{C}HOOH$ radicals.

An estimate of the internal and translational energies of the important chain-branching intermediate HPMF shows that while most of the internal and translational energy is in the vibrational modes of the HPMF (∼59%), this energy is on average only about 17 kcal/mol above zero-point energy for HPMF and may be insufficient for unimolecular decomposition of HPMF, which requires surmounting barriers of at least 42 kcal/mol. Interestingly, the •OH has ∼20% of the estimated internal and translational energy in translation (the second highest energy partition after the vibrational energy of HPMF). Since the breaking of the O−O bond involves the translation of the •OH, it is not surprising that the •OH translational energies are somewhat correlated with the lifetime of $HOOCH_2O\dot{C}HOOH$, exhibiting a possible trimodal distribution as in the characteristic decay times shown in Figure 6. We caution that the 70 trajectories from b-TS1 do not represent an exhaustive sampling of the phase space for this system, and further trajectories are required to confirm the observations made here.

Last, we investigated the unimolecular decomposition of HPMF starting from the b-TS2, b-TS5, and b-TS5′ transition states (see Figure 11). The latter two types of trajectories did not yield any unusual dynamics over 1 ps, but the former trajectories through b-TS2 did yield unexpected short-time dynamics. The decomposition of HPMF through b-TS2 to form HC(═O)OH + HĊO + •OH is endothermic (∼39 kcal/mol), and the reverse reaction to re-form HPMF has a barrier of only ∼7 kcal/mol. In the 30 trajectories started from b-TS2, a loose complex of HC(═O)OH and HĊOOH is formed, which in six trajectories (20%) recross b-TS2 to re-form HPMF. In 10 trajectories (33%), the HC(═O)OH, HĊO, and •OH fully separate. Because of unfavorable thermodynamics (see Table 3), one must consider these products as kinetically controlled. However, in the remaining 14 trajectories (47%), the loose complex of HC(═O)OH and HĊOOH rearranges to form products that are more thermodynamically favorable than HC(═O)OH + HĊO + •OH. These products include formic acid anhydride (FAA; HC(═O)OC(═O)H) + $H_2O$, HC(═O)OH + CO + $H_2O$, HC(═O)OH + HC(═O)OH, and $CH_2OO$ + HC(═O)OH. All of these stable products except for $CH_2OO$ have been observed in (hydrogenated) DME combustion experiments.[33,35] Rearrangements of unstable products from HPMF decomposition may need to be taken into account for more quantitative kinetics modeling of the stable product ratios presented in the experimental work of Curran et al.[33] and Liu et al.[35] Though many more trajectories would be needed to establish definitive branching ratios for these products (and

reveal any other possible rearrangements of HC(═O)OH and HĊOOH), these results are suggestive that the unimolecular decomposition HPMF does not exclusively form unstable radical species such as •OH, •$OCH_2OC$(═O)H, HĊO, and $CH_2OO$ that are ready for further bimolecular reactions. These radicals can be attracted by other fragments in the HPMF unimolecular decomposition process and produce thermodynamically stable species, thereby potentially stifling further oxidation of the DME fuel. This is not a prediction that could have been made with simple statistical rate theories.

The inhibition of further reaction of the DME chain branching intermediate HPMF by both the recrossing of b-TS1 from $HOOCH_2O\dot{C}HOOH$ to •$OOCH_2OCH_2OOH$ via hydrogen transfer and by the rearrangement of HĊO + •OH + HC(═O)OH to form thermodynamically more stable products represent dynamic mechanisms that may limit production of •OH. With a diminished supply of •OH (i.e., less than two •OH per consumed DME molecule), first-stage DME autoignition due to chain branching is expected to be somewhat hindered.

**Acknowledgment.** A.A. and E.A.C. thank Drs. D. J. Mann, E. W. Kaiser, and W. F. Schneider and Mr. J. J. Szente for helpful discussions. Funding for this work was provided by the Ford Motor Company. We are pleased to contribute this chemical dynamics article in honor of Prof. Bill Hase, a true chemical dynamics pioneer.

**Supporting Information Available:** A table of DFT-B3LYP/6-31G** frequencies and zero-point vibrational energy for the deuterated species considered in this study. This material is available free of charge via the Internet at http://pubs.acs.org.

## References and Notes

(1) Kitamura, T.; Ito, T.; Senda, J.; Fujimoto, H. *JSAE Rev.* **2001**, *22*, 139−145.

(2) Sorenson, S. C. *Trans. ASME* **2001**, *123*, 652−657 and references therein.

(3) Curran, H. J.; Pitz, W. J.; Westbrook, C. K.; Dagaut, P.; Boettner, J.-C.; Cathonnet, M. *Int. J. Chem. Kinet.* **1998**, *30*, 229−241.

(4) Andersen, A.; Carter, E. A. *Isr. J. Chem.* **2002**, *42*, 245−260.

(5) Andersen, A.; Carter, E. A. *J. Phys. Chem. A* **2003**, *107*, 9463−9478.

(6) Herron, J. T.; Huie, R. E. *J. Am. Chem. Soc.* **1977**, *99*, 5430.

(7) Herron, J. T.; Huie, R. E. *Int. J. Chem. Kinet.* **1978**, *10*, 1019.

(8) Atkinson, R.; Aschmann, S. M.; Arey, J.; Shorees, B. *J. Geophys. Res.* **1992**, *97*, 6065.

(9) Atkinson, R.; Tuazon, E. C.; Aschmann, S. M. *Environ. Sci. Technol.* **1995**, *29*, 1860.

(10) Niki, H.; Maker, P. D.; Savage, C. M.; Breitenbach, L. P.; Hurley, M. D. *J. Phys. Chem.* **1987**, *91*, 941.

(11) Atkinson, R.; Aschmann, S. M. *Environ. Sci. Technol.* **1993**, *27*, 1357.

(12) Donahue, N. M.; Kroll, J. H.; Anderson, J. G.; Demerjian, K. L. *Geophys. Res. Lett.* **1997**, *25*, 59−62.

(13) Bach, R. D.; André, J. L.; Owensby, A. L.; Schlegel, H. B.; McDouall, J. J. W. *J. Am. Chem. Soc.* **1992**, *114*, 7207.

(14) Cremer, D.; Schidt, T.; Gauss, J.; Radhakrishnan, T. P. *Angew. Chem., Int. Ed. Engl.* **1988**, *27*, 427.

(15) Gremer, D.; Gauss, J.; Kraka, E.; Stanton, J. F.; Bartlett, R. J. *Chem. Phys. Lett.* **1993**, *209*, 547.

(16) Wadt, W. R.; Goddard, W. A., III. *J. Am. Chem. Soc.* **1975**, *97*, 3004.

(17) Harding, L. B.; Goddard, W. A., III. *J. Am. Chem. Soc.* **1978**, *100*, 7180.

(18) Su, F.; Calvert, J. G.; Shaw, J. H. *J. Phys. Chem.* **1980**, *84*, 239−246.

(19) Martinez, R. I.; Herron, J. T. *J. Environ. Sci. Health* **1981**, *A16*, 623−636.

(20) Hatakeyama, S.; Bandow, H.; Okuda, M.; Akimoto, H. *J. Phys. Chem.* **1981**, *85*, 2249.

(21) Niki, H.; Maker, P. D.; Savage, C. M.; Breitenbach, L. P. *J. Phys. Chem.* **1981**, *85*, 1024−1027.

(22) Kan, C. S.; Su, F.; Calvert, J. G.; Shaw, J. H. *J. Phys. Chem.* **1981**, *85*, 2359.

(23) Hatakeyama, S.; Kobayashi, H.; Akimoto, H. *J. Phys. Chem.* **1984**, *88*, 4736.

(24) Hatakeyama, S.; Kobayashi, H.; Lin, Z.; Tagaki, H.; Akimoto, H. *J. Phys. Chem.* **1986**, *90*, 4131.

(25) Neeb, P.; Horie, O.; Moortgat, G. K. *Int. J. Chem. Kinet.* **1996**, *28*, 721.

(26) Thamm, J.; Wolff, S.; Turner, W. V.; Gäb, S.; Thomas, W.; Zabel, F.; Fink, E. H.; Becker, K. H. *Chem. Phys. Lett.* **1996**, *258*, 155−158.

(27) Wolff, S.; Boddenberg, A.; Thamm, J.; Turner, W. V.; Gäb, S. *Atmos. Environ.* **1997**, *31*, 2965−2969.

(28) Aplincourt, P.; Ruiz-López, M. F. *J. Phys. Chem. A* **2000**, *104*, 380−388.

(29) Aplincourt, P.; Ruiz-López, M. F. *J. Am. Chem. Soc.* **2000**, *122*, 8990−8997.

(30) Borckholtz, T.; Andersen, A.; Carter, E. A. Manuscript in preparation.

(31) Sehested, J.; Møgelberg, T.; Wallington, T. J.; Kaiser, E. W.; Nielsen, O. J. *J. Phys. Chem.* **1996**, *100*, 17218−17225.

(32) Maricq, M. M.; Szente, J. J.; Hybl, J. D. *J. Phys. Chem. A* **1997**, *101*, 5155−5167.

(33) Curran, H. J.; Fischer, S. L.; Dryer, F. L. *Int. J. Chem. Kinet.* **2000**, *32*, 741−759.

(34) Dagaut, P.; Daly, C.; Simmie, J. M.; Cathonnet, M. The oxidation and ignition of dimethyl ether from low to high temperature (500−1000 K) experiments and kinetic modeling. In *Twenty-Seventh Symposium (International) on Combustion*; The Combustion Institute: Pittsburgh, PA, 1998.

(35) Liu, I.; Cant, N. W.; Bromly, J. H.; Barnes, F. J.; Nelson, P. F.; Haynes, B. S. *Chemosphere* **2001**, *42*, 583−589.

(36) Bolton, K.; Hase, W. L.; Peslherbe, G. H. Direct Dynamics Simulations of Reactive Systems. In *Modern Methods for Multidimensional Computation in Chemistry*; Thompson, D. L., Ed.; World Scientific: Hackensack, NJ, 1998 and references therein.

(37) Doubleday, C., Jr.; Bolton, K.; Hase, W. L. *J. Phys. Chem. A* **1998**, *102*, 3648−3658.

(38) Doubleday, C., Jr.; Bolton, K.; Peslherbe, G. H.; Hase, W. L. *J. Am. Chem. Soc.* **1996**, *118*, 9922.

(39) Doubleday: C.; Nendel, M.; Houk, K. N.; Thweatt, D.; Page, M. *J. Am. Chem. Soc.* **1999**, *121*, 4720−4721.

(40) Stephens, P. J.; Devlin, F. J.; Chabalowski, C. F.; Frisch, M. J. *J. Phys. Chem.* **1994**, *98*, 11623−11627.

(41) Hehre, W. J.; Ditchfield, R.; Pople, J. A. *J. Chem. Phys.* **1972**, *56*, 2257−2261.

(42) Hariharan, P.; Pople, J. *Theor. Chim. Acta* **1973**, *28*, 213.

(43) Francl, M.; Petro, W.; Hehre, W. J.; Binkley, J.; Gordon, M.; Defrees, D.; Pople, J. *J. Chem. Phys.* **1982**, *77*, 3654−3665.

(44) Jaguar v4.1, Schrödinger, Inc.: Portland, OR, 2000.

(45) Krishnan, R.; Binkley, J. S.; Seeger, R.; Pople, J. A. *J. Chem. Phys.* **1980**, *72*, 650−654.

(46) Pople, J.; Gill, P.; Handy, N. *Int. J. Quantum Chem.* **1995**, *56*, 303.

(47) Jensen, F. *Introduction to Computational Chemistry*; John Wiley & Sons: Chichester, England, 1999.

(48) Curtiss, L. A.; Raghavachari, K.; Redfern, P. C.; Pople, J. A. *J. Chem. Phys.* **1997**, *106*, 1063−1079.

(49) Andersen, A.; Carter, E. A. To be published.

(50) Bartlett, R. J. *J. Phys. Chem.* **1989**, *93*, 1697.

(51) Curtiss, L. A.; Raghavachari, K.; Trucks, G. W.; Pople, J. A. *J. Chem. Phys.* **1991**, *94*, 7221−7230.

(52) Ochterski, J. W.; Petersson, G. A.; Montgomery, J. A., Jr. *J. Chem. Phys.* **1996**, *104*, 2598−2619.

(53) Hase, W. L. Classical Trajectory Simulations: Initial Conditions. In *Encyclopedia of Computational Chemistry*; Schleyer, P. v. R.; Allinger, N. L.; Clark, T.; Gasteiger, J.; Kollman, P. A.; Schaefer, H. F., III; Schreiner, P. R., Eds.; Wiley: New York, 1998.

(54) Peslherbe, G. H.; Wang, H.; Hase, W. L. Adv. Chem. Phys.: Monte Carlo sampling for classical trajectory simulations. In *Monte Carlo Methods in Chemical Physics*; Ferfuson, D. M.; Siepmann, J. I.; Truhlar, D. G., Eds.; John Wiley & Sons: New York, 1999; Vol. 105 and references therein.

(55) McQuarrie, D. A. *Statistical Thermodynamics*; University Science Books: Mill Valley: CA, 1973.

(56) Bunker, D. L. *Methods Comput. Phys.* **1971**, *10*, 287.

(57) Forst, W. *Theory of Unimolecular Reactions*; Academic Press: New York, 1973.

(58) Peña-Gallego, A.; Martinez-Nuñez, E.; Vázquez, S. A. *Phys. Chem. Chem. Phys.* **2000**, *2*, 5393−5399.

(59) Swope, W. C.; Andersen, H. C.; Berens, P. H.; Wilson, K. R. *J. Chem. Phys.* **1982**, *76*, 637.

(60) Hodges, Matthew P. XMakemol version 5.05, 2002.

(61) Grace-5.1.0. 1991−1995, Paul J. Turner, Portland, OR; 1996−2003, Grace Development Team.

(62) Steffens, K. L.; Luque, J.; Jeffries, J. B.; Crosley, D. R. *J. Chem. Phys.* **1997**, *106*, 6262−6267.
(63) Hase, W. L.; Duchovic, R. J.; Swamy, K. N.; Wolf, R. J. *J. Chem. Phys.* **1984**, *80*, 714−719.
(64) Holbrook, K. A.; Pilling, M. J.; Robertson, S. H. *Unimolecular Reactions*, 2nd ed.; John Wiley & Sons: Chichester, England, 1996.
(65) Gilbert, R. G.; Smith, S. C. *Theory of Unimolecular and Recombination Reactions*; Blackwell Scientific Publications: Oxford, England, 1990.
(66) Steinfeld, J. I.; Fransciso, J. S.; Hase, W. L. *Chemical Kinetics and Dynamics*; Prentice Hall: Englewood Cliffs, NJ, 1989.
(67) Bunker, D. L.; Hase, W. L. *J. Chem. Phys.* **1973**, *59*, 4621.
(68) Rynbrandt, J. D.; Rabinovitch, B. S. *J. Chem. Phys.* **1971**, *75*, 2164.
(69) Doubleday: C. *J. Phys. Chem. A* **2001**, *105*, 6333−6341.
(70) Lu, D.; Hase, W. L. *J. Phys. Chem.* **1988**, *92*, 3217−3225.
(71) Martínez-Núñez, E.; Marques, J. M. C.; Vázquez, S. A. *J. Chem. Phys.* **2001**, *115*, 7872−7880.
(72) Varandas, A. J. C.; Marques, J. M. C. *J. Chem. Phys.* **1992**, *96*, 5137.
(73) Ben-Nun, M.; Levine, R. D. *J. Chem. Phys.* **1994**, *101*, 8768.
(74) Lim, K. F.; McCormack, D. A. *J. Chem. Phys.* **1995**, *102*, 1705.
(75) Forsythe, K. M.; Gray, S. K.; Klippenstein, S. J.; Hall, G. E. *J. Chem. Phys.* **2001**, *115*, 2134−2145.
(76) NIST Standard Reference Database 69, March 2003 Release; NIST Chemistry WebBook.
(77) Guthrie, J. P. *J. Am. Chem. Soc.* **1974**, *96*, 3608−3615.
(78) $\Delta H_f$(298 K) for formoxyl ($HCO_2$) calculated from the $\Delta H_{rxn}$(298 K) of $HCO_2$ dissociating to $CO_2$ and H derived from DFT-B3LYP/6-311G** total energies, zero-point vibrational energies (ZPVE) and $C_p$(298 K)'s for $HCO_2$, H, and $CO_2$ (−6.5 kcal/mol) calculated by us and known experimental $\Delta H_f$(298 K)'s for H (52.1 kcal/mol) and $CO_2$ (−94.1 kcal/mol) from the NIST Standard Reference Database 69, March 2003 Release; NIST Chemistry WebBook.
(79) Frank, I.; Parrinello, M.; Klamts, A. *J. Phys. Chem. A* **1998**, *102*, 3614−3617.
(80) Chase, M. W., Jr. *J. Phys. Chem. Ref. Data* **1998**, *9*, 1−1951 (4th ed.).